# Glycolipid Biosurfactant as Multilamellar Vesicular Drug Carriers

Silvia Alonso-De-Castro, Chloé Seyrig, Korin Ozkaya, Julien Dumond, Luisa Riancho, Javier Perez, Christophe Hélary, Niki Baccile

**HAL Id: hal-03399740**

**https://hal.science/hal-03399740**

Preprint submitted on 24 Oct 2021

# Glycolipid Biosurfactant as Multilamellar Vesicular Drug Carriers

Silvia Alonso-de-Castro,[a] Chloé Seyrig,[a] Korin Ozkaya[a], Julien Dumond,[b] Luisa Riancho,[c] Javier Perez,[d] Christophe Hélary[a,*], Niki Baccile[a,*]

[a] Sorbonne Université, Centre National de la Recherche Scientifique, Laboratoire de Chimie de la Matière Condensée de Paris, LCMCP, F-75005 Paris, France

[b] Centre interdisciplinaire de recherche biologique, Collège de France, 75005 Paris, France

[c] Centre de Recherche INSTITUT DE LA VISION, UMR_S968 Inserm / UPMC / CHNO des Quinze-Vingts, 75012, Paris, France

[d] Synchrotron Soleil, L'Orme des Merisiers, Saint-Aubin, BP48, 91192 Gif-sur-Yvette Cedex, France

**Abstract**

Microbial amphiphiles, known as biosurfactants, are molecules obtained fermentation of yeasts or bacteria. Biobased and biodegradable, they have been historically developed for detergency formulations, whereas more recent work has shown their interest as antimicrobials or depollutants. However, their self-assembly properties and their interactions with macromolecules suggest a broader potential of applications. Drug encapsulation for anti-cancer purposes is a well-known application of lipids such as phospholipids. In this study, for the first time, a drug delivery system based on microbial amphiphiles is designed and tested against human cervical carcinoma HeLa cells. For this purpose, multilamellar wall vesicles (MLWV) consisting of microbial glucolipid (GC) amphiphiles and polylysine (PLL), attracted by electrostatic interactions, have been synthesized. Curcumin, a highly lipophilic molecule, has been used as natural drug model to evaluate the GCPLL MLWVs as potential nanocarrier to specifically deliver drugs into cancer cells. The curcumin loaded MLWVs uptake measured by flow cytometry is much higher in Hela cells (50%) compared to NHDF (35%) and THP-1 derived macrophages (20%). This uptake is correlated to cytotoxicity as cell viability only decreases for Hela cells (by 50%). A dedicated mechanistic study shows that the cytotoxic effect is based on MLWV fusion with the cell membrane and the curcumin release within the cellular cytoplasm. Taken together, these results demonstrate that

microbial amphiphiles can be used to develop engineered drug delivery system to efficiently target cancer cells.

**Introduction**

Biological amphiphiles, sometimes referred to as biosurfactants, are molecules produced by microorganisms and developed for their high ecosustainable profile.[1] Among the different families of biosurfactants available (glycolipids, lipoproteins or lipopeptides, polymeric), glycolipids are certainly the most relevant one for their high-throughput production process and broadness of applications. In particular, their use in the biomedical field[2] has long been reported, but is mainly focused on the development of antibiotics.[2] In the pharmacological field, there have been reports[3,4] on the anticancer properties of specific microbial glycolipids (e.g., sophorolipids) since 2008,[5] but these results are still under debate.[6] Biosurfactants-based carriers have been proposed in the past years,[7] but in the best case scenario, the main lipidic vehicle is generally constituted by a classical phospholipid liposome.[8,9] Hence, a better understanding of the effects of biosurfactants on pre-formed bilayer membranes,[10–12] thus making the liposomal vector is necessary to obtain more complex particles. In the several cases, the lipid particle formation leads to an uncontrolled structure.[13]

The analysis of the self-assembly properties of microbial glycolipids[14,15] has opened the opportunity to conceive phospholipid-free stimuli-responsive complex colloidal structures, only composed of bioamphiphiles. Multilamellar wall vesicles (MLWV), belonging to the family of polyelectrolyte-surfactant complexes (PESC), are interesting colloids, originally employed in gene transfection,[16] for which the stability is generally considered better than single-wall vesicles. In recent reports, we have controlled the attractive electrostatic interactions between microbial C18:1-*cis* single-glucose lipid (G-C18:1, **GC**, Figure 1) and poly-L-lysine (**PLL**) at the micelle-to-vesicle phase transition of **GC** and shown the formation of phospholipid-free, stable, MLWV.[17,18] The multilamellar wall structure is composed of alternating layers of GC and PLL and is prepared from a pH-stimulated phase transition in water around pH 7.[17] Indeed, microbial glycolipids in general, and **GC** in particular, have a curious asymmetric bolaform structure with a free-standing COOH group, making the molecule pH-sensitive with a more complex phase behavior than classical lipids or surfactants.

Drug delivery systems are engineered technologies which allow the targeting and/or the controlled release of active principles. They overcome several drawbacks related to the systemic administration of free pharmacological molecules such as side effects, drug solubility, stability in biological environment, rapid clearance or non-specific delivery, etc.[19] Thus, the therapeutic index of a pharmacological drug can be improved

thanks to drug delivery technologies. These systems are often in the form of a drug carrier, which specifically distributes and protects the active principle from degradation and removal by the reticuloendothelial system (RES).[19]

Several examples of such delivery systems have been extensively reported in the literature, which include liposomes,[20] polymers[21] and polymeric micelles,[22] peptide based biomaterials,[23] inorganic nanoparticles,[24] and gels among others.[25] Liposomes are the most common form, investigated as nanocarriers for drug encapsulation. They have a characteristic bilayer assembly mimicking the cellular membrane, are easy-to-prepare and bio-compatible.[20] Despite their benefits, liposomes also face several drawbacks, such as the reticuloendothelial clearance and/or immune response.[26] A similar behavior has been reported for PEGylated constructs with an augmented immune response after several doses.[26] Therefore, there is an emergent and continuous need to discover alternatives for drug delivery strategies to overcome such issues.

In this perspective, it is of particular interest to evaluate engineered MLWV composed of glycolipid biosurfactant and biocompatible polyelectrolyte as a carrier of hydrophobic, as well as hydrophilic, drugs. Both small hydrophilic and hydrophobic drugs have been widely demonstrated that are effective against several diseases, but their therapeutic effect can be limited by the rapid clearance from the systemic circulation or a local site of administration, lipophilicity and therefore lower bioavailability.[27,28] In this study, the drug-loading and targeting potential of MLWV composed of GC and PLL (**GCPLL** MLWV) is evaluated towards mouse fibroblasts L929, normal human dermal fibroblasts NHDF, macrophages derived THP-1 and human cervical carcinoma HeLa. For this purpose, the encapsulation and mechanism of released curcumin, the active component of *Curcuma longa* plant, which combines lipophilicity, fluorescence but also anticancer properties, are analyzed.[29,30] In addition **GCPLL** MLWV carriers are also evaluated to deliver other commercial drugs with different degree of lipophilicity.

**Experimental**

The experimental section is given in the Supporting Information file.

**Results and discussion**

*GCPLL MLWVs are stable in cell culture medium*

Multilamellar wall vesicles only composed of glycolipid biosurfactant **GC** (Figure 1) and polyelectrolyte **PLL** have been previously reported to form in mQ-grade water below pH ~ 7.5.[17,18] Study of their formation in cell culture medium is then a necessary

108   step to develop carriers for biological applications. A typical cell culture medium contains

109   a wide variety of compounds such as salts, glucose and amino acids, but also proteins

110   coming from the supplemented Fetal Bovine Serum (FBS). Such a physicochemical

111   complexity may alter the charge, composition and/or the pH-range of stability of **GCPLL**

112   MLWV. This latter is prepared by pH modulation as described elsewhere,[17,18] except for

113   the replacement of water by FBS supplemented DMEM cell culture medium.

114       SAXS experiments using synchrotron radiation performed during the pH-

115   controlled synthesis process provide the necessary real-time structural information

116   proving the existence of multilamellar structure of the nanocarriers.[17] pH-resolved *in*

117   *situ* synchrotron SAXS is then performed on the GCPLL system from alkaline to acidic

118   pH in DMEM and the corresponding contour plot between q= 0.1 and 0.4 $\text{Å}^{-1}$ is shown in

119   Figure 1a.

120       Below pH 8 and approximately until pH ~5, two sharp diffraction peaks

121   correspond to the first ($q_{(001)}$) and second ($q_{(002)}$) order reflections ($q_{(001)}$= 0.171 $\text{Å}^{-1}$, $q_{(002)}$=

122   0.341 $\text{Å}^{-1}$) of the multillamelar wall vesicles MLWV phase (Figure 1a), evolving during pH

123   decrease. This is in full agreement with our previous observations in water.[17,18] Below

124   pH ~5, a structural gap at $q_{(001)}$ reveals the previously-reported transition between MLWV

125   and a PLL-free lamellar phase composed of **GC** only, characterized by a peak at q=

126   0.169 $\text{Å}^{-1}$.[17] Previously, it was shown that **GCPLL** MLWVs synthesized in $H_2O$ are stable

127   at a pH ranging from 4 to ~7.5 (2.5 mg/mL), the exact extreme pH values however

128   depending on experimental conditions, like the **GC**-to-**PLL** ratio and possibly the salt

129   content.[17,18] The present experiment shows that the use of DMEM cell culture medium

130   does not influence at all the formation of **GCPLL** MLWV and it even seems that the

131   domain of pH stability may even be increased to higher pH values  (~8) than in pure

132   water (~7.5) (Figure 1a). Variations in the limits of the pH transition are not unexpected

133   and they can be qualitatively explained as follows. **GCPLL** MLWV are stabilized by

134   attractive electrostatic forces between negatively-charged **GC** and positively-charged

135   **PLL**. If both NMR and ITC experiments have shown that most negative charges are

136   compensated by positive charges,[17] the exact amount of both negative and positive

137   charges varies with pH and ionic strength for both **GC** and **PLL**. In pure water and

138   absence of added salt, the optimal balance of charges for the MLWV phase starts at pH

139   ~7.5; in DMEM, rich in salt, one expects that the optimal charge balance occurs at higher

140   pH, when part of the higher content of negative charges are counterbalanced by the free

141   cations in solution.

142       Being multilamellar systems, MLWVs are birefringent under polarized light.[18]

143   Polarized light microscopy (PLM, Figure 1b and Figure S1) images are obtained under

144   white (b1) and polarized light (b2 and b3) with polarizers at 0°-90° and 45°-135°

respectively. PLM reveals the presence of vesicular structures displaying optical birefringence in the shape of typical maltese cross, colocalized with the vesicle, in agreement with previous work.[18] PLM thereby confirms both the vesicular shape and multilamellar wall structure of **GCPLL** colloids in solution.
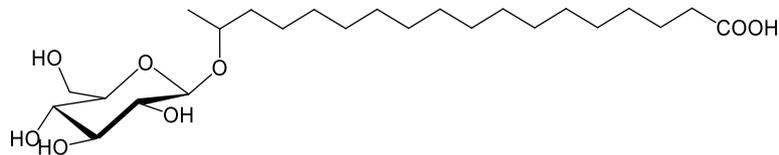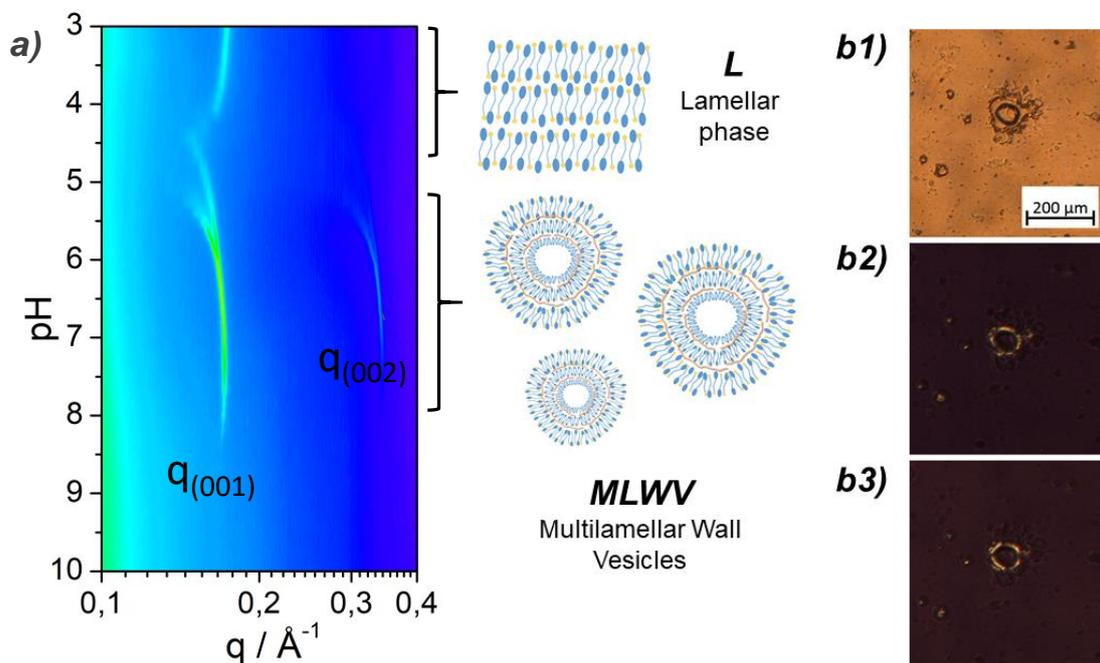




**Figure 1. a) Graphical representation of SAXS at different pH values of 2.5 mg/ml of G-C18:1PLL (1:1) in DMEM cell culture medium, where L: Lamellar phase and MLWV: multilamellar wall vesicles.  b1) PLM images of GCPLL 2.5 mg/mL in DMEM cell culture medium containing birefringent patterns on the surface evidenced by rotation of the polarizers from 45°–135° (b2) to 0–90°(b3)**

Quantitative $^1$H solution NMR, using methanol-$d_4$ as common solvent, is employed to determine the content of **GC** and **PLL** within MLWVs compared to a reference standard TMSP-$d_4$. $^1$H NMR spectra show that **GCPLL** MLWVs in H$_2$O (pH= 5.5) have a molar ratio of molecules consisting of 6.5 % of the initial content of **PLL** and 70% of the initial content of GC. Otherwise, when **GCPLL** MLWVs are prepared in DMEM

163  cell culture medium (pH = 7.4), one observes a proportional decrease of both **PLL** and
164  **GC** molar ratios, 4 and 45 % respectively (Table 1 and Figures S2-S5). A reduced
165  content of both **GC** and **PLL** in DMEM with respect to water samples agrees well with
166  the higher pH at which MLWV formation occurs. As previously measured by SAXS
167  (Figure 1a), MLWVs in DMEM are formed in the pH range 4.5-8, whereas pH 8
168  constitutes the upper pH limit above which MLWV start to disassemble. It is reasonable
169  to suppose that for pH values close to the limit of pH 8, part of the MLWV have started
170  to disassemble and the composition decreases. This issue could be easily solved by
171  adapting the initial content of **GC** and **PLL**, but this was out of the scope of this work. All
172  in all, this structural analysis shows that the **GCPLL** MLWV prepared as such can be
173  used for biological applications at physiological pH in culture medium. In addition, the
174  final molar ratio $GC_f/PLL_f$ in $H_2O$ and DMEM after preparation of MLWV remains
175  practically constant (57 and 60 respectively). The ratio between COOH and $NH_2$
176  functional groups, partially reflecting the charge ratio, is given in Table 1 as
177  [COOH]/[$NH_2$] and one respectively finds 2.8 and 3 for $H_2O$ and DMEM, concluding that
178  the composition of MLWVs is comparable independently of the nature of the aqueous
179  medium.

180

181  **Table 1. Quantitative evaluation of G-C18:1 (GC) and PLL in MLWV by ^{1}H Solution NMR.**
182  **Explanation of the calculation is described in Table S1.**

|  | $C_{initial}$ (mM) | | $C_{final}$ (mM) | | $C_F/C_{In}$ (%) | | Molar ratio | | Functional group |
|---|---|---|---|---|---|---|---|---|---|
|  | [GC]$_{in}$ | [PLL]$_{in}$ | [GC]$_f$ | [PLL]$_f$ | GC$_{f/in}$ | PLL$_{f/in}$ | GC$_{in}$/ PLL$_{in}$ | GC$_f$/ PLL$_f$ | [COOH]/ [$NH_2$] |
| $H_2O$ | 5.4 | 1 | 3.7 | 0.065 | 70 | 6.5 | 5.4 | 57 | 2.8 |
| DMEM | 5.4 | 1 | 2.4 | 0.04 | 45 | 4 | 5.4 | 60 | 3 |

183

184

185  *GCPLL MLWVs less cytotoxic than GC alone*

186       The cytotoxicity of **GCPLL** MLWVs is not known. This parameter is evaluated in
187  mouse fibroblasts L929 cell line by dilution of the initial 2.5 mg/mL mixture to obtain
188  different concentrations (range from 0 to 1 mg/ml). All the concentrations are referred to
189  as the initial quantity employed in the preparation. As controls, the viability of cells is
190  evaluated after incubation with **GC** and **PLL** independently, as well as the medium at the
191  same pH. The latter corresponds to a **GC**- and **PLL**-free DMEM medium which has
192  undergone the same pH changes required to prepare **GCPLL** MLWVs. These results
193  are shown in Figures S6, S7.

**PLL** and pH medium controls show no significant cytotoxic effect under the studied conditions. On the contrary, **GC** (Figure S7) has a significant impact on the L929 viability, as only 80 % of the control metabolic activity is measured when $C_{GC}$= 250 µg/mL is used and dramatically decreases to less than 10% from 500 µg/mL on. Regarding **GCPLL** MLWVs, a cytotoxic effect is observed from 250 µg/mL as the metabolic activity drops to 60%. From 500 µg/mL, only 20% of cells are alive (Figure S6). However, no significant cytotoxicity is observed with $C_{GCPLL}$= 100 µg/mL.

According to the ^{1}H solution NMR analysis (Figure S2-5 and Table S1), about 95 % of free PLL and 50% of free GC are detected in a **GCPLL** colloidal solution fabricated with DMEM cell culture medium. For this reason, we suspect that most of the cytotoxic effect of the **GCPLL** solution is associated to free **GC** molecules. We then develop an alternative strategy to evaluate the cell viability without the presence of extra **GC** free molecules in solution. **GCPLL** MLWVs are prepared in DMEM as described previously,[18] but they are centrifuged at 3000 rpm for 5 min, then the supernatant is discarded (thus eliminating the free forms of **GC** and **PLL**) and replaced by the same volume of fresh DMEM, prior to their analysis and further use. The **GCPLL** pellet is resuspended by vortexing and sonicating for few seconds, recovering its initial colloidal stability.[18] The latter is most likely explained by surface charge arguments, an important physicochemical parameter that influences the colloidal stability of the suspensions. The zeta-potential of **GCPLL** MLWVs in cell culture medium is fund to be of -11.9 ± 0.4 mV, meaning that **GCPLL** MLWVs have a slight negative surface charge, which may prevent aggregation.[31,32]

The cell viability measured after incubation with **GCPLL** MLWVs after centrifugation is presented in Figure S6, now showing no significant cytotoxity of **GCPLL** MLWVs up to 250 µg/mL in L929 mouse fibroblast cell line, while the as-prepared MLWVs containing free **GC** exhibits a viability of about 50%. This result confirms that the cytotoxic effect previously found for **GCPLL** MLWVs is essentially attributable to the free **GC** in solution. Finally, Figure S7 shows no cytotoxicity associated to the controls, that is **PLL** and DMEM, the latter undergone with pH changes as described above. The cytotoxicity of **GCPLL** MLWVs is eventually assessed on several cell lines (blue bars on Figure 2): macrophages derived THP-1, Normal Human Dermal fibroblasts and Hela cells. The concentration range settles within the range contained between 20 and 1000 µg/mL, comparable to other drug delivery systems, such as loaded and blank liposomes.[33–35]
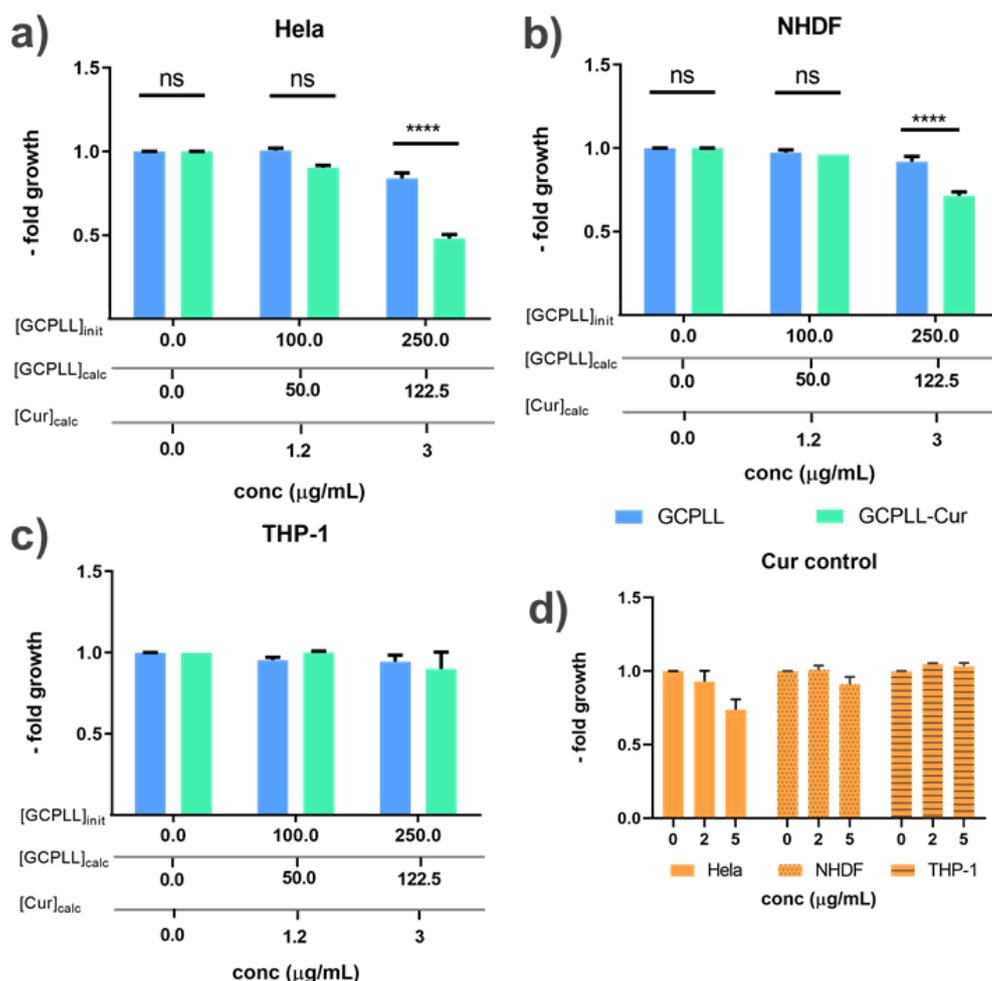
**Figure 2. a-c) Cell viability of GCPLL (blue), GCPLL-Cur (green) in a) Hela cells; b) NHDF cells; and c) THP-1 cells. Three abscissa are displayed from a) to c) to show the initial concentration employed in the MLWVs preparation, the calculated GCPLL content and the Cur encapsulated. In particular, [GCPLL]$_{init}$ refers to concentrations employed initially in the preparation of GCPLL; [GCPLL]$_{calc}$ refers to concentrations calculated by $^1$H NMR (Table 1) after centrifugation and resuspension of the MLWVs pellet; and [Cur]$_{calc}$ refers to the encapsulated Cur in the MLWVs measured by UV-Vis (Figure 3). d) Cell viability of Curcumin control in the three different cell types tested.**

*Curcumin is efficiently encapsulated within MLWVs*

The multilamellar lipid structure, the stability of **GCPLL** MLWVs in physiological culture medium and their absence of cytotoxicity make them ideal candidates as phospholipid-free drug delivery system based on biological amphiphiles alone. MLWVs may combine the advantages of drug loading capacity, biodegradability, and biocompatibility based on biosurfactants obtained from microbial source.

Curcumin, the active component of *Curcuma longa* plant, is a molecule widely used as drug due to its antioxidant, anti-inflammatory and anticancer properties.[29,36] Curcumin (**Cur**) is highly lipophilic, with a water-octanol partition coefficient, logP, in the order of 2.6 and a membrane partition constant above $10^4$ $M^{-1}$.[30] Similarly to other hydrophobic drugs,[37] curcumin has limited applicability due to its poor oral bioavailability, low chemical stability[38] as well as its weak cellular uptake.[29] As a consequence, the accumulation of curcumin is low within the cytoplasm.[39,40] The cell uptake process of curcumin has been reported to penetrate the cell membrane and interact with the lipids of the membrane through H-bonding and hydrophobic interactions. Different strategies could be followed to overcome these limitations, such as the synthesis of curcumin derivatives,[29] or the development of drug delivery systems to enhance the stability and increase its cellular uptake. [41]

Therefore, curcumin was chosen as model natural drug to load the **GCPLL** system with the aim of probing the encapsulation capacity of MLWVs and to show their potential to enhance the therapeutic index of the encapsulated drug curcumin.



c)

$$Loading\ Capacity\ (LC\ \%) = \frac{Curcumin\ encapsulated}{GCPLL\ weight} \times 100 = 2.5\ \%$$

$$Encapsulation\ Efficiency\ (EE\ \%) = \frac{Curcumin\ encapsulated}{Curcumin\ loaded} \times 100 = 60\ \%$$
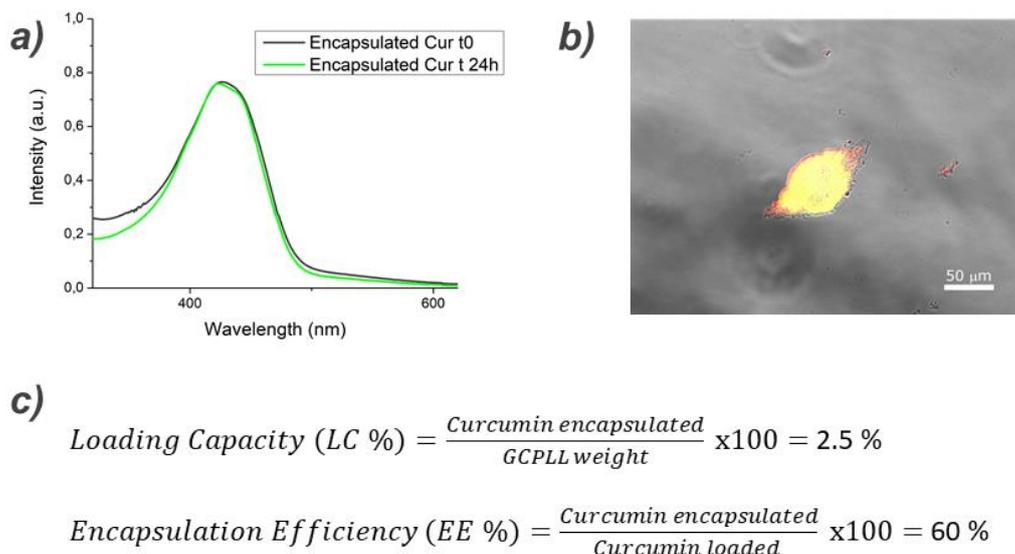
**Figure 3. a) UV-Vis spectra of Curcumin encapsulated in GCPLL at t= 0 and t= 24h in DMEM cell culture medium. GCPLL-Cur is centrifuged out and resuspended in ethanol for analysis. b) Fluorescence microscopy image of GCPLL-Rhod-Cur at 2.5 mg/mL in DMEM cell culture medium. Liss-Rhod (red) and Curcumin (green) are loaded within particles. c) Calculation of Loading capacity (LC%) and Encapsulation Efficiency (EE%), where the amount of Cur encapsulated is 30 µg, the loaded quantity 50 µg and the weight of GCPLL 1225 µg considering the values obtained from ^{1}H NMR evaluation (Table1).**

270

The process of curcumin (**Cur**) encapsulation is based on a straightforward and fast mixture and vortexing protocol described in the experimental section in the Supporting Information. Addition of **Cur** does not modify the zeta potential of **GCPLL-Cur** MLWVs, which is -13.2 ± 0.3 mV, thus justifying the colloidal stability after resuspension.

UV-vis absorbance measurements are performed to quantify the **Cur** encapsulated in **GCPLL** MLWVs just after fabrication and after 24 hours of incubation in culture medium. (Figure 3a). These experiments involve dissolution of the **GCPLL-Cur** MLWVs pellet in ethanol, a common solvent for all components. The absorption spectra are superimposable, thereby showing that **Cur** is stable within the MLWVs aqueous solution over 24 h. In addition, this result shows that **Cur** is encapsulated in **GCPLL** in its native form. This can be considered as a crucial advantage compared to free **Cur** in solution. Indeed, it has been reported that **Cur** decomposes approximately by 50% in cell culture medium supplemented with 10% serum after 8 hours of incubation.[42] The encapsulated concentration corresponds to 80 µM **Cur**, and this concentration is calculated using the calibration curve reported in Figure S8.

To exclude coprecipitation and to confirm that **Cur** is actually colocalized in the **GCPLL** MLWVs, we perform fluorescence microscopy on a drop of **GCPLL-Cur** MLWVs solution. **GCPLL** MLWVs are simultaneously labelled with rhodamine using a rhodamine-modified C18:1 lipid (Liss-Rhod PE), known to intercalate in the glucolipid membrane without interfering with the structure for lipid-to-dye molar ratio above 200.[43] The colocalized fluorescence, red for Liss-Rhod PE and green for **Cur** as well as the DIC white light for GCPLL confirm the encapsulation of **Cur** within MLWVs, rather than coprecipitation (Figure 3b). Colocalization of **Cur** (green) and Liss-Rhod PE (red) is also demonstrated within the cellular compartment, as shown and discussed later.

A key parameter to characterize drug delivery systems is the encapsulation efficiency (EE %), defined in the formula given in Figure 3c. EE % is sensitive to different properties related to each system such as morphology, hydrophobicity, charge of the surface, permeability, the structure of the encapsulated molecule as well as the encapsulation process.[44,45] Taking into account the molar concentration of **Cur** obtained by UV-Vis (80 µM) and the total loaded Cur (135 µM), one can then calculate the drug loading of this system and finds EE% = 60%. This value is higher than other EE% estimated for other vesicular systems, which show a high variability, ranging from 1 to 68% for vesicles and 6 to 31% for multilamellar vesicles (MLV).[46] The broad spectrum of reported EE % values between unilamellar vesicles (ULVs) and MLVs is commonly explained by the presence of a lumen in ULVs, allowing a higher loading volume of drug

307    compared to the actual lipid content.[46] Despite the structure differences, we have
308    reached comparable EE % in MLVs compared to ULVs.

309        The loading capacity (LC %, Figure 3c) is defined as the ratio between the
310    amount of **Cur** encapsulated (30 µg) and the weight of GCPLL system calculated by $^1$H
311    NMR (1225 µg). The loading capacity that we obtain for **GCPLL-Cur** is about 2.5%
312    (Figure 3c). In the present case, the two-step preparation protocol of **GCPLL-Cur** may
313    explain the low LC % value: considering that MLWVs are already formed when **Cur** is
314    added, encapsulation may occur only in the outer layers of the MLWVs. The strong
315    discrepancy between LC % and EE % may confirm this hypothesis: the drug is mainly
316    encapsulated in the outer lipid layer of the MLWVs, which would involve a good
317    encapsulation process but a low drug-to-lipid content. Different protocols could probably
318    improve both the EE and LC% of Cur, but this is out of the scope of the present work.

319

320    *Curcumin is selectively delivered to HeLa cells via a membrane-fusion mechanism*

321        The antiproliferative activity of curcumin loaded MLWVs is explored in three
322    different human cell lines (Figure 2a-c): Normal Dermal Human Fibroblasts (NHDF),
323    cervical carcinoma HeLa cells and THP-1 monocyte-derived macrophages.

324        HeLa cells are chosen as model to evaluate the **GCPLLs** as drug carriers to
325    target cancer cells, i.e with high proliferative activities. On the opposite, NHDF are used
326    as model of normal cells with moderate proliferative activities to assess the effect of
327    MLWVs with regards to the multiplication potential. Last, THP1 derived macrophages
328    are used in this study to evaluate the targeting of **GCPLL** toward cancer cells.
329    Macrophages are members of the reticulo endothelial system (RES) and possess high
330    phagocytic activities to clear particles from the human body. Concentrations in Figure
331    2a-c are given as [GCPLL]$_{init}$, i.e the initial GCPLL concentrations, and [GCPLL]$_{calc}$ and
332    [Cur]$_{calc}$, the concentrations of GCPLL and curcumin, respectively, calculated after
333    removal of free GC by centrifugation.

334        First of all, free **Cur** control (Figure 2d) has no toxic effect on THP-1 derived
335    macrophages (orange/line bar) and NHDF (orange/dotted bar) and it only slightly
336    reduces cell viability of Hela cells for the 5 µg/mL concentration (orange bar). Similarly,
337    the **GCPLL** (blue bar) control has no cytotoxic effect neither on THP-1 (Figure 2c)
338    derived macrophages nor on NHDF (Figure 2b), with a slight reduction in cell viability
339    (>80 %) on the HeLa cells for the highest concentration tested (Figure 2a), that is 250
340    µg/mL but corresponding to 122.5 µg/mL after centrifugation. Finally, the curcumin-
341    loaded MLWV system, **GCPLL-Cur** (green bar), has no effect on the THP-1 (Figure 2c),
342    for 100 and 250 µg/mL (initial concentrations), and NHDF (Figure 2b) up 100 µg/mL,
343    while a slight cytotoxicity is measured at 250 µg/mL (cell viability at about 75%),

respectively of calculated concentrations of 50 and 122.5 µg/mL. Regarding the HeLa cancer cell line (Figure 2a), a dramatic effect (50% cell viability) is observed for **GCPLL-Cur** at the highest concentration, when compared to the maximum **Cur** content in the control experiment (Figure 2d, 75% cell viability) and **GCPLL** controls (Figure 2c). The cytotoxic effect of **GCPLL-Cur** is higher than the one of free curcumin despite a lower cargo: the calculated curcumin content in the most toxic **GCPLL-Cur** sample (50% cell viability) is about 3 µg/mL, while the curcumin control displays a 75% viability at curcumin concentration of 5 µg/mL.

As the cytotoxic effect of curcumin encapsulated within **GCPLL** MLWVs is greater in Hela cells compared to NHDF and macrophages, it seems to be positively correlated with the proliferative rate of cells. Indeed, cancer cells such Hela possess a very short doubling time, NHDF have moderate proliferative activities and macrophages derived THP-1 do not proliferate.

Liposomal curcumin systems applied in pharmacology,[35] in particular the studies of Huang *et al.*[47] employed carboxymethyl dextran (CMD) modifiying liposomal curcumin in Hela cells, reporting an $IC_{50}$ of 6.6 µM, and in another study by Saengkrit *et al.*[48] involving curcumin loaded cationic liposomes showed $IC_{50}$ in Hela and SiHa cells of 21 µM and 16 µM, respectively. In comparison with our results, we employed 8.1 µM loaded curcumin in MLWVs to reach 50 % cytotoxicity in Hela cells (Figure 2c), which is comparable to CMD $IC_{50}$ in Hela cells, but much better than the liposomes based system.

These results put in evidence the remarkable activity of **GCPLL-Cur** MLWVs towards cancer cell line HeLa, with little cytotoxic effect in both normal cells, i.e fibroblasts and no dividing cells such as macrophages, thus avoiding the potential damage in normal tissue and the clearance by the reticuloendothelial system (RES), which is dedicated for the foreign particles elimination. Cytotoxicity of curcumin encapsulated within GCPLL MLWVs seems to be correlated, on one side, with the proliferative rate of cells, and on the other side, with the encapsulation efficiency. They are highly toxic for cancer cells which possess a high doubling time but not on no dividing cells such as macrophages.
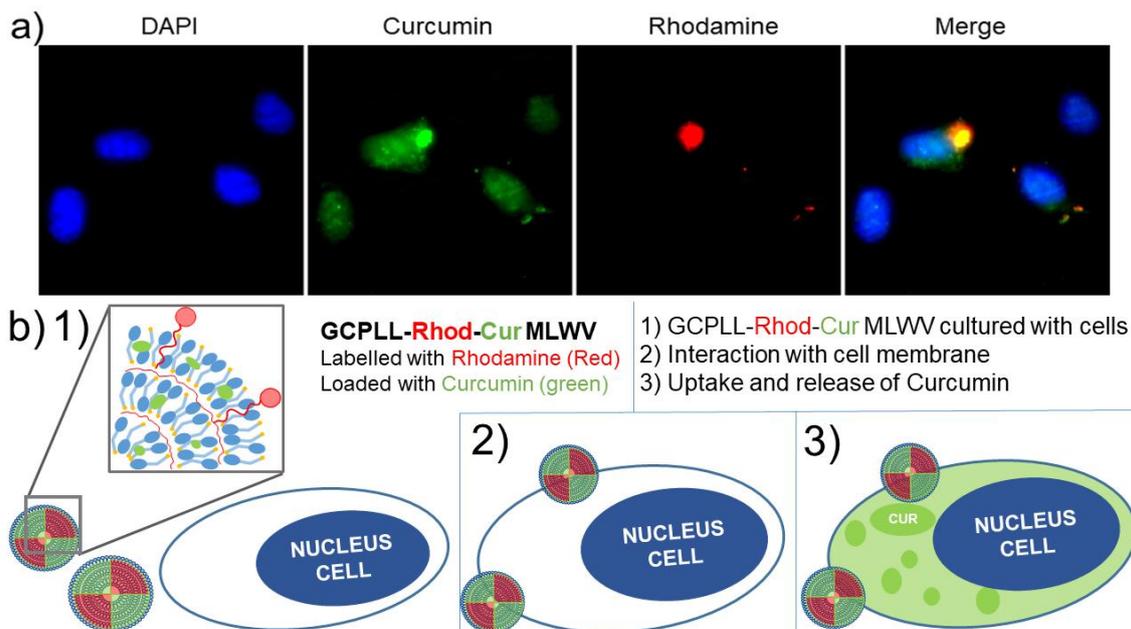
**Figure 4. a) Fluorescence microscopy images on HeLa cells treated with GCPLL-Cur 100 µg/ml and nucleus stained in blue with DAPI, green fluorescence from Curcumin, red from rhodamine and the merged image of the three channels. b) Schematic representation of the uptake mechanism of GCPLL-Rhod-Cur.**

To better understand the mechanism of action of the **GCPLL-Cur** MLWVs on HeLa cells, we couple fluorescence (Figure 4) and confocal microscopy (Figure 5, Figures S9-15) with flow cytometry (Figure 5, Figures S16-18). Figure 4a shows three fluorescence microscopy images, each corresponding to different channels: the nucleus (stained with DAPI, blue), **Cur** (green) and **GCPLL** (stained with rhodamine, red). All channels are eventually combined in a fourth image (merge).

Colocalization of curcumin and rhodamine (yellow) in the merge image and presence of green curcumin around the blue nucleus demonstrate the mechanism of cell uptake occurring in Hela cells. **GCPLL** MLWVs labelled with rhodamine (Liss-Rhod) and loaded with **Cur** penetrate into the cell membrane and **Cur** is eventually released within the cytoplasm. At the same time, no red fluorescence signal alone is detected inside the cell, meaning that **GCPLL** MLWVs fuse with the cell membrane and deliver **Cur** within the the cytoplasm. A schematic representation of the uptake mechanism is illustrated in Figure 4b.

Figures S9-15 in the supporting information show the fluorescence microscopy images of Hela, NHDF and THP-1 cells with the corresponding images for control, Cur alone (with and without Liss-Rhod), **GCPLL** (and **GCPLL-Rhod**) and **GCPLL-Cur** (and **GCPLL-Cur-Rhod**). It is worth noticing that fluorescent grains are observed within Hela

13

398     cells when they are incubated with **GCPLL**-**Cur** (Figure S11 and S12, green) and

399     **GCPLL**-**Cur**-**Rhod** (Figure S13, red and overlapped green and red respectively). On the

400     opposite, a blurry and weak green fluorescence is detected when free curcumin is used

401     (Figure S11). This shows an accumulation of curcumin within Hela cells when GCPLL

402     particles are used, thereby evidencing their efficacy to deliver drugs inside the cancer

403     cells. This effect is specific as no granny fluorescence is detected in NHDF or

404     macrophages derived THP-1 (Figure S9, S10, S14, S15).

405        Confocal microscopy imaging in Figure 5a shows images of Hela, NHDF and

406     THP-1 cells incubated with GCPLL-Cur-Rhod and nucleus stained with DAPI. In addition

407     to Hela cells, both planes *yz* and *zx* were included (Figure S19), which confirms the

408     proposed mechanism: **GCPLL** labelled with rhodamine (red) is localized in the outer part

409     of the cell while **Cur** (green) is released in the cytoplasm of the HeLa cells (Figure 5a)

410     and it surrounds the nucleus (blue).

411        Flow cytometry measurements of the three different cell lines tested (THP-1,

412     NHDF, and Hela) are presented in Figure 5b and in the Supporting Information (Figure

413     S16-18) and they evidence different uptake quantities of the MLWVs by measuring the

414     intensity of rhodamine in cells. The results demonstrate that HeLa cells have the highest

415     percentage of rhodamine labelling (41% for **GCPLL-Rhod** and 50% for **GCPLL-Rhod-**

416     **Cur**), which explains the higher uptake, and therefore higher cytotoxicity, compared to

417     both THP-1 and NHDF, which respectively show a rhodamine signal of 20% and 34%

418     for **GCPLL-Rhod-Cur**.

419        The lipid-based particles can be uptaken by the cells following different cellular

420     mechanisms. Nanoparticles ranging from 50-100 nm can be engulfed by endocytosis,

421     those less than 400 nm by micropinocytosis and micrometric particles can enter the cells

422     by phagocytosis.[49] The latter phenomenon is dedicated to immune cells of the

423     reticuloendothelial system such as macrophages and neutrophils. The curcumin loaded

424     MLWVs are poorly engulfed by macrophages, thereby showing phagocytosis is not

425     involved in the intracellular delivery of curcumin. The MLWVs population is quite

426     polydisperse ranging from 10 nm up to 10 μm. A fraction of particles could be uptaken

427     by macropinocytosis. However, no rhodamine fluorescence, evidencing the presence of

428     micropinocytosis vesicles, is observed within the cellular cytoplasma of NHDF and Hela

429     cells. Hence, the major mechanism of curcumin delivery seems to be based on MLWVs

430     fuse with the cell membrane. This fusion is much easier in dividing cells as their lipid

431     membrane is more fluid and favors MLWVs interaction. Particle interaction with dividing

432     cells does not seem to depend on the cell doubling time as Hela and NHDF exhibit the

433     same quantity of cells labeled with rhodamine, as quantified by FACS (Figure 5b).

434     However, the quantity of curcumin delivered within Hela cells is much larger than that in

435 normal fibroblasts (Figure 5a). Hence the process of fusion is favored by the proliferative
436 activities of cells, which is an asset to target and kill cancer cells. Curcumin toxicity has
437 been improved by its encapsulation in GCPLL MLWVs compared to the free form despite
438 a smaller quantity as the loading efficiency does not exceed 60%.
439     In addition to FACS and fluorescence microscopy, cell viability results correlate
440 to the higher fluorescence detected of the uptaken Curcumin in Hela cells than in NHDF
441 (Figure 5a), demonstrating a higher toxicity in Hela cells than in NHDF cells (Figure 2).



442
443

b)

| Flow cytometry | Hela | NHDF | THP-1 |
|---|---|---|---|
| GCPLL-Rhod | 26.4 ± 0.6 % | 46.8 ± 2.0 % | 15.3 ± 10 % |
| GCPLL-Rhod-Cur | 41.8 ± 9.2 % | 33.3 ± 3.0 % | 15.8 ± 8.7 % |

444
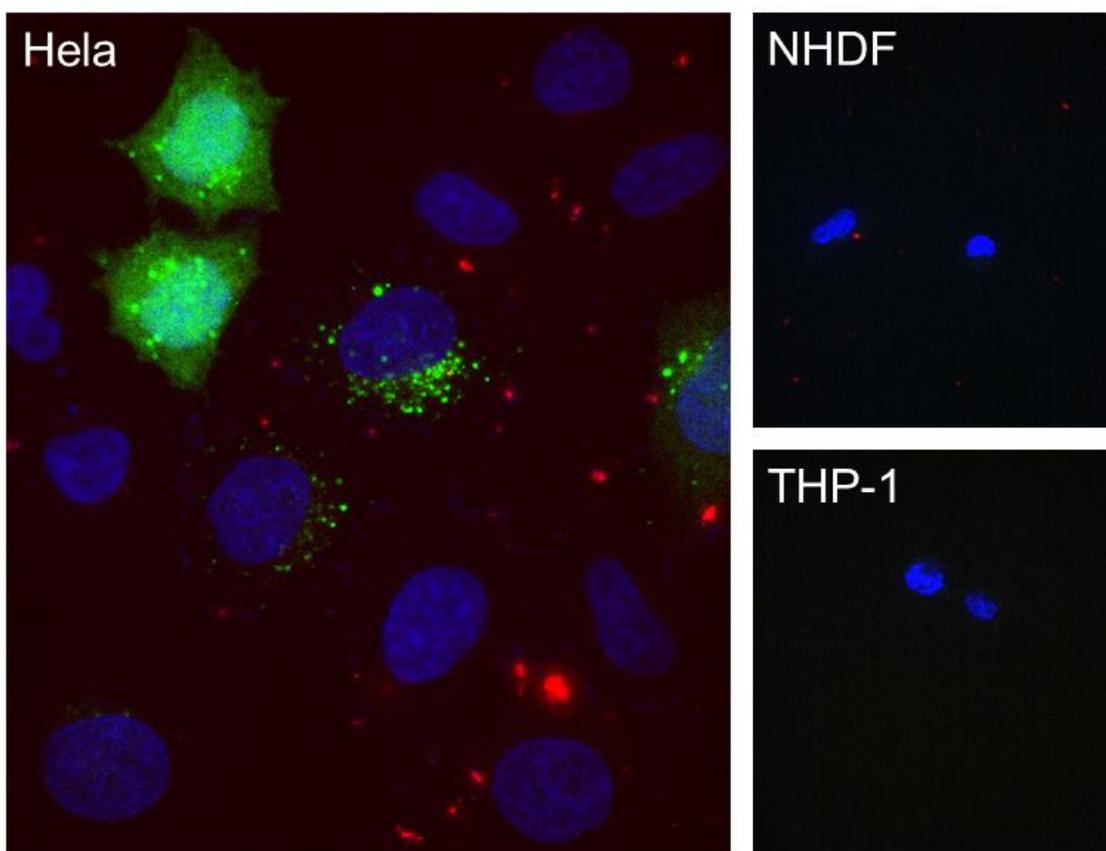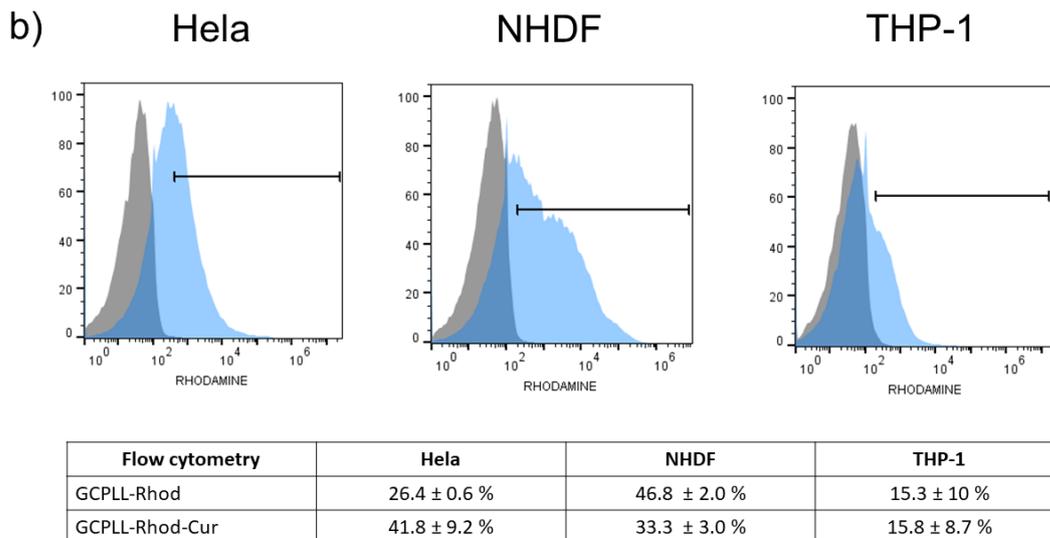
**Figure 5. a) Confocal microscopy images of Hela, NHDF and THP-1 cells treated with GCPLL-Rhod-Cur 100 µg/mL. Color code: green= Curcumin, red= rhodamine –stained GCPLL MLWV, blue= cell nucleus. b) Flow cytometry FACS data of Hela, NHDF and THP-1 cells of incubated with 100 µg/mL GCPLL and GCPLL-Cur labelled with Liss-Rhod. Table with mean ± SD values of triplicate of triplicates of GCPLL and GCPLL-Cur both labelled with Liss-Rhod for the three cell lines tested.**

In order to extend the encapsulation feasibility of this MLWV system with a wider variety of drugs which display a different hydrophobic character, we screened the **GCPLL** encapsulation and cell cytotoxicity of Doxorubicin (logP = 1.41),[50] Paclitaxel (logP = 3)[51] and Docetaxel (logP = 2.4)[52] in Hela and NHDF cells (Table 2).

Results demonstrated the possibility to exploit the MLWVs with other encapsulated small molecules which provoked a higher cytotoxic effect preferentially over Hela cells than in NHDF for all encapsulated drug types tested. In the case of Doxorubicin (Dox), there is a great decrease in viability reaching 26.8 ± 1.6% at 250 µg/mL GCPLL-Dox, compared to empty GCPLL 89 ± 3% in Hela cells, while in NHDF cells there is a slighter decrease in viability being 69.2 ± 0.9% at 250 µg/mL GCPLL-Dox. For Paclitaxel and Docetaxel, both GCPLL loaded systems at 250 µg/mL showed a cell viability higher than 65% in NHDF cells. On the contrary, in Hela cells the effect is again increased compared with analogous NHDF experiments. GCPLL-Pac at 250 µg/mL is 59.3 ± 0.5% and GCPLL-Doc at 250 µg/mL is 44.3 ± 1.3%. In these last two systems, it is observed a milder effect in the cytotoxicity compared with Doxorubicin experiments.

| Cell viability ± SEM (%) | Hela cells | | NHDF cells | |
|---|---|---|---|---|
| | 100 µg/mL | 250 µg/mL | 100 µg/mL | 250 µg/mL |
| GCPLL | 93.3 ± 6.9 | 89.5 ± 3.0 | 95.9 ± 2.9 | 98.7 ± 1.3 |
| GCPLL-DOX | 66.9 ± 1.8 | 26.8 ± 1.7 | 81.3 ± 1.4 | 69.3 ± 0.9 |
| GCPLL-PAC | 98.7 ± 1.2 | 59.3 ± 0.6 | 91.6 ± 5.6 | 77.7 ± 6.2 |
| GCPLL-DOC | 79.5 ± 8.1 | 44.3 ± 1.3 | 85.5 ± 4.2 | 67.0 ± 2.0 |

468

469 **Table 2. Cell viability data of three different drug experiment tested in Hela and**
470 **NHDF cells treated with prepared concentrations 100 µg/mL (50 µg/mL) and 250**
471 **µg/mL (125 µg/mL) of: GCPLL, GCPLL-drug. Being the drugs tested: Doxorubicin**
472 **(DOX), Paclitaxel (PAC) and Docetaxel (DOC). Table with mean ± SEM values of**
473 **triplicate of triplicates.**

474

475 **Conclusions**

476      This work demonstrates that microbial amphiphile biosurfactants can be
477 used as drug carriers in the absence of phospholipid addition. Control over the
478 self-assembly properties of microbial glucolipid **GC** in the presence of polylysine
479 **PLL** shows the possibility to form **GCPLL** vesicle colloids with multilamellar wall
480 (MLWVs), both in water and DMEM culture medium. **GCPLL** particles are stable
481 at physiological pH, as their multilamellar structure is probed both by *in situ* SAXS
482 measurements and polarized light microscopy.

483      With the aim of evaluating **GCPLL** as novel drug delivery system,
484 curcumin, used as lipophilic drug model have been efficiently encapsulated within
485 **GCPLL**. Curcumin loaded **GCPLL** (encapsulation efficiency of 60 %) shows a
486 greater therapeutic effect towards cancer Hela cells compared to free curcumin,
487 with a decrease of Hela viability by 50 % for an encapsulated content of 3 µg/mL
488 **GCPLL-Cur**. Beside, this decrease is only of 25% the free curcumin
489 concentration at 5 µg/mL. In addition, this cytotoxic impact is exclusive to cancer
490 cells, as no significant effect is observed on normal human dermal fibroblasts
491 NHDF and THP-1 derived macrophages. This suggests that **GCPLL-Cur** MLWVs
492 would avoid side effects. In addition, this system would increase the circulation
493 time of therapeutic drugs in the bloodstream since **GCPLL** are not engulfed by
494 macrophages, cells in charge of the clearance of foreign particles *in vivo*. Last,
495 analyses by confocal microscopy and flow cytometry show that curcumin is
496 delivered within the cell by **GCPLL-Cur** fusion with the Hela membrane.

Taken together, these results demonstrate that vesicle-forming biosurfactant amphiphiles, glucolipids in this work, but possibly rhamnolipids, sophorolipid-derivatives or surfactin, can be employed as novel multilamellar vescicular systems for drug delivery, thus broadening the use of this class of compounds to more high-end applications.

**References**

1. Desai, J. D. & Banat, I. M. Microbial production of surfactants and their commercial potential. *Microbiol. Mol. Biol. Rev.* **61**, 47–64 (1997).

2. Rodrigues, L. R. & Teixeira, J. A. Biomedical and therapeutic applications of biosurfactants. *Adv. Exp. Med. Biol.* **672**, 75–87 (2010).

3. Haque, F., Khan, M. S. A. & AlQurashi, N. ROS-Mediated Necrosis by Glycolipid Biosurfactants on Lung, Breast, and Skin Melanoma Cells. *Front. Oncol.* **0**, 253 (2021).

4. Thakur, P. *et al.* Rhamnolipid the Glycolipid Biosurfactant: Emerging trends and promising strategies in the field of biotechnology and biomedicine. *Microb. Cell Factories 2021 201* **20**, 1–15 (2021).

5. Fu, S. L. *et al.* Sophorolipids and Their Derivatives Are Lethal Against Human Pancreatic Cancer Cells. *J. Surg. Res.* **148**, 77–82 (2008).

6. Callaghan, B. *et al.* Lactonic sophorolipids increase tumor burden in Apcmin+/- mice. *PLoS One* **11**, 1–16 (2016).

7. Rodrigues, L. R. Microbial surfactants: Fundamentals and applicability in the formulation of nano-sized drug delivery vectors. *J. Colloid Interface Sci.* **449**, 304–316 (2015).

8. Nakanishi, M., Inoh, Y., Kitamoto, D. & Furuno, T. Nano vectors with a biosurfactant for gene transfection and drug delivery. *J. Drug Deliv. Sci. Technol.* **19**, 165–169 (2009).

9. Sanches, B. C. P. *et al.* Rhamnolipid-based liposomes as promising nano-carriers for enhancing the antibacterial activity of peptides derived from bacterial toxin-antitoxin systems. *Int. J. Nanomedicine* **16**, 925–939 (2021).

10. Ortiz, A. *et al.* Interactions of a bacterial biosurfactant trehalose lipid with phosphatidylserine membranes. *Chem. Phys. Lipids* **158**, 46–53 (2009).

11. Ortiz, A. *et al.* Effects of a bacterial trehalose lipid on phosphatidylglycerol membranes. *Biochim. Biophys. Acta - Biomembr.* **1808**, 2067–2072 (2011).

12. Otzen, D. E. Biosurfactants and surfactants interacting with membranes and proteins: Same but different? *Biochim. Biophys. Acta - Biomembr.* **1859**, 639–

649 (2017).

13. Müller, F. *et al.* Rhamnolipids form drug-loaded nanoparticles for dermal drug delivery. *Eur. J. Pharm. Biopharm.* **116**, 31–37 (2017).

14. Baccile, N. *et al.* Self-Assembly Mechanism of pH-Responsive Glycolipids: Micelles, Fibers, Vesicles, and Bilayers. *Langmuir* **32**, 10881–10894 (2016).

15. Baccile, N. *et al.* Self-assembly, interfacial properties, interactions with macromolecules and molecular modelling and simulation of microbial bio-based amphiphiles (biosurfactants). A tutorial review. *Green Chem.* **23**, 3842–3944 (2021).

16. Safinya, C. R. Structures of lipid-DNA complexes: Supramolecular assembly and gene delivery. *Curr. Opin. Struct. Biol.* **11**, 440–448 (2001).

17. Seyrig, C. *et al.* Stimuli-induced non-equilibrium phase transitions in polyelectrolyte-surfactant complex coacervates. *Langmuir* **36**, 8839–8857 (2020).

18. Seyrig, C., Griel, P. Le, Cowieson, N., Perez, J. & Baccile, N. Synthesis of multilamellar walls vesicles polyelectrolyte-surfactant complexes from pH-stimulated phase transition using microbial biosurfactants. *J. Colloid Interface Sci.* **580**, 493–502 (2020).

19. Majumder, J. & Minko, T. Multifunctional and stimuli-responsive nanocarriers for targeted therapeutic delivery. *Expert Opin. Drug Deliv.* **18**, 205–227 (2021).

20. Filipczak, N., Pan, J., Yalamarty, S. S. K. & Torchilin, V. P. Recent advancements in liposome technology. *Adv. Drug Deliv. Rev.* **156**, 4–22 (2020).

21. Kopeček, J. & Yang, J. Polymer nanomedicines. *Advanced Drug Delivery Reviews* vol. 156 40–64 (2020).

22. Hwang, D., Ramsey, J. D. & Kabanov, A. V. Polymeric micelles for the delivery of poorly soluble drugs: From nanoformulation to clinical approval. *Adv. Drug Deliv. Rev.* **156**, 80–118 (2020).

23. Varanko, A., Saha, S. & Chilkoti, A. Recent trends in protein and peptide-based biomaterials for advanced drug delivery. *Advanced Drug Delivery Reviews* vol. 156 133–187 (2020).

24. Luther, D. C. *et al.* Delivery of drugs, proteins, and nucleic acids using inorganic nanoparticles. *Advanced Drug Delivery Reviews* vol. 156 188–213 (2020).

25. Jain, K. K. An Overview of Drug Delivery Systems. in *Drug Delivery Systems. Methods in Molecular Biology* vol. 2059 1–54 (Humana Press Inc., 2020).

26. Sercombe, L. *et al.* Advances and challenges of liposome assisted drug delivery. *Frontiers in Pharmacology* vol. 6 286 (2015).

27. Senapati, S., Mahanta, A. K., Kumar, S. & Maiti, P. Controlled drug delivery

570        vehicles for cancer treatment and their performance. *Signal Transduct. Target.*
571        *Ther. 2018 31* **3**, 1–19 (2018).

572  28.  Li, Q., Li, X. & Zhao, C. Strategies to Obtain Encapsulation and Controlled
573        Release of Small Hydrophilic Molecules. *Front. Bioeng. Biotechnol.* **0**, 437
574        (2020).

575  29.  Tomeh, M. A., Hadianamrei, R. & Zhao, X. A review of curcumin and its
576        derivatives as anticancer agents. *International Journal of Molecular Sciences*
577        vol. 20 (2019).

578  30.  Heger, M., Golen, R. F. Van, Broekgaarden, M. & Michel, M. C. The Molecular
579        Basis for the Pharmacokinetics and Pharmacodynamics of Curcumin and Its
580        Metabolites in Relation to Cancer. *Pharmacol. Rev.* **66**, 222–307 (2014).

581  31.  Patil, S., Sandberg, A., Heckert, E., Self, W. & Seal, S. Protein adsorption and
582        cellular uptake of cerium oxide nanoparticles as a function of zeta potential.
583        *Biomaterials* **28**, 4600–4607 (2007).

584  32.  Puttipipatkhachorn, S., Nunthanid, J., Yamamoto, K. & Peck, G. E. Drug physical
585        state and drug-polymer interaction on drug release from chitosan matrix films. *J.*
586        *Control. Release* **75**, 143–153 (2001).

587  33.  Nandi, U., Onyesom, I. & Douroumis, D. An in vitro evaluation of antitumor
588        activity of sirolimus-encapsulated liposomes in breast cancer cells. *J. Pharm.*
589        *Pharmacol.* **73**, 300–309 (2021).

590  34.  Wang, W. *et al.* Flexible liposomal gel dual-loaded with all-trans retinoic acid and
591        betamethasone for enhanced therapeutic efficiency of psoriasis. *J.*
592        *Nanobiotechnology* **18**, (2020).

593  35.  Feng, T., Wei, Y., Lee, R. J. & Zhao, L. Liposomal curcumin and its application in
594        cancer. *Int. J. Nanomedicine* **12**, 6027–6044 (2017).

595  36.  Goel, A., Kunnumakkara, A. B. & Aggarwal, B. B. Curcumin as 'Curecumin':
596        From kitchen to clinic. *Biochem. Pharmacol.* **75**, 787–809 (2008).

597  37.  Kalepu, S. & Nekkanti, V. Insoluble drug delivery strategies: Review of recent
598        advances and business prospects. *Acta Pharmaceutica Sinica B* vol. 5 442–453
599        (2015).

600  38.  Quitschke, W. W. Differential solubility of curcuminoids in serum and albumin
601        solutions: Implications for analytical and therapeutic applications. *BMC*
602        *Biotechnol.* **8**, 84 (2008).

603  39.  Barry, J. *et al.* Determining the effects of lipophilic drugs on membrane structure
604        by solid-state NMR spectroscopy: The case of the antioxidant curcumin. *J. Am.*
605        *Chem. Soc.* **131**, 4490–4498 (2009).

606  40.  Tsukamoto, M., Kuroda, K., Ramamoorthy, A. & Yasuhara, K. Modulation of raft

607   domains in a lipid bilayer by boundary-active curcumin. *Chem. Commun.* **50**,
608   3427–3430 (2014).

609 41. Karthikeyan, A., Senthil, N. & Min, T. Nanocurcumin: A Promising Candidate for
610   Therapeutic Applications. *Front. Pharmacol.* **0**, 487 (2020).

611 42. Wang, Y. J. *et al.* Stability of curcumin in buffer solutions and characterization of
612   its degradation products. *J. Pharm. Biomed. Anal.* **15**, 1867–1876 (1997).

613 43. Ben Messaoud, G. *et al.* Single-Molecule Lamellar Hydrogels from Bolaform
614   Microbial Glucolipids. *Soft Matter* **16**, 2528–2539 (2020).

615 44. Nicholas, A. R., Scott, M. J., Kennedy, N. I. & Jones, M. N. Effect of grafted
616   polyethylene glycol (PEG) on the size, encapsulation efficiency and permeability
617   of vesicles. *Biochim. Biophys. Acta - Biomembr.* **1463**, 167–178 (2000).

618 45. Kulkarni, S. B., Betageri, G. V. & Singh, M. Factors affecting microencapsulation
619   of drugs in liposomes. *J. Microencapsul.* **12**, 229–246 (1995).

620 46. Sun, B. & Chiu, D. T. Determination of the encapsulation efficiency of individual
621   vesicles using single-vesicle photolysis and confocal single-molecule detection.
622   *Anal. Chem.* **77**, 2770–2776 (2005).

623 47. Huang, Q. *et al.* Coating of carboxymethyl dextran on liposomal curcumin to
624   improve the anticancer activity. *RSC Adv.* **4**, 59211–59217 (2014).

625 48. Saengkrit, N., Saesoo, S., Srinuanchai, W., Phunpee, S. & Ruktanonchai, U. R.
626   Influence of curcumin-loaded cationic liposome on anticancer activity for cervical
627   cancer therapy. *Colloids Surfaces B Biointerfaces* **114**, 349–356 (2014).

628 49. Manzanares, D. & Ceña, V. Endocytosis: The Nanoparticle and Submicron
629   Nanocompounds Gateway into the Cell. *Pharm. 2020, Vol. 12, Page 371* **12**, 371
630   (2020).

631 50. Doxorubicin hydrochloride | DrugBank Online.

632 51. Paclitaxel: Uses, Interactions, Mechanism of Action | DrugBank Online.

633 52. Docetaxel: Uses, Interactions, Mechanism of Action | DrugBank Online.

634

# Supporting Information

# Glycolipid Biosurfactant as Multilamellar Vesicular Drug Carriers

Silvia Alonso-de-Castro,[a] Chloé Seyrig,[a] Korin Ozkaya[a], Julien Dumond,[b] Luisa Riancho,[c] Javier Perez,[d] Christophe Hélary[a],*, Niki Baccile[a],*

[a] Sorbonne Université, Centre National de la Recherche Scientifique, Laboratoire de Chimie de la Matière Condensée de Paris, LCMCP, F-75005 Paris, France

[b] Centre interdisciplinaire de recherche biologique, Collège de France, 75005 Paris, France

[c] Centre de Recherche INSTITUT DE LA VISION, UMR_S968 Inserm / UPMC / CHNO des Quinze-Vingts, 75012, Paris, France

[d] Synchrotron Soleil, L'Orme des Merisiers, Saint-Aubin, BP48, 91192 Gif-sur-Yvette Cedex, France

## Experimental

### Materials

Microbial glycolipids G-C18:1 are made of a single *β*-D-glucose hydrophilic headgroup and a C18 fatty acid tail (monounsaturation in position 9,10). The syntheses of glycolipid G-C18:1 is described in Ref. [1], where the typical ^{1}H NMR spectra and HPLC chromatograms are given. The compound used in this work have a molecular purity of more than 95%. Poly-L-lysine (PLL) hydrobromide ($M_w \approx$ 1-5 KDa, p$K_a$ ~10-10.5)[2] is purchased from Sigma-Aldrich. All other chemicals are of reagent grade and are used without further purification. Curcumin (Cur) is purchased from Sigma-Aldrich without further purification. 18:1 Liss Rhod PE: 1,2-dioleoyl-sn-glycero-3-phosphoethanolamine-N-(lissamine rhodamine B sulfonyl) (ammonium salt) (Liss-Rhod) ($M_w$= 1301.7 g/mol, $\lambda_{abs}$= 560 nm, $\lambda_{em}$= 583 nm) is purchased from Avanti lipids. Lipopolysacharides (LPS), Phorbol 12-myristate 13-acetate (PMA), paraformaldehyde (PFA), Docetaxel, Paclitaxel and Doxorubicin are purchased from Sigma Aldrich-Merck. DAPI (4',6-Diamidino-2-Phenylindole, Dihydrochloride) is purchased from Life Technologies-ThermoFisher Scientific.

### Cell culture

L929 (mouse fibroblast) cells (Merck), HeLa (human cervical carcinoma) cells and NHDF (Normal human dermal fibroblast) (Merck) cells are cultured in Dulbecco's Modified Eagle Medium (DMEM) supplemented with 10% fetal bovine serum (FBS) and 1% penicillin/streptomycin and 1% Anphotericin B. THP-1 (human monocyte) (Promocell) cells are cultured in RPMI 1640 medium supplemented with 10% fetal bovine serum (FBS) and 1% penicillin/streptomycin and 1% Amphotericin B. Cells are cultivated at 37°C and 5% $CO_2$ under 100% humidity.

### Preparation G-C18:1-PLL (*GCPLL*) multilamellar wall vesicles (MLWVs)

**GCPLL** MLWVs are prepared according to previous work.[3,4] Stock solutions are prepared by dissolving 5 mg of **GC** or PLL in 1 mL of DMEM cell culture medium supplemented with 10 % FBS. Both solutions are raised to pH 10 with NaOH 1 M, a step necessary to solubilize **GC** (micellar phase), and mixed in a 1:1 volume ratio, followed by vortexing. The final concentration of **GC** and **PLL** is 2.5 mg/mL. pH is then lowered to 7 with HCl 1 M to trigger MLWVs formation. The solution is slightly cloudy at pH 7, confirming the presence of MLWVs colloids.[3,4]

*Encapsulation of curcumin (**Cur**) in GCPLL (**GCPLL-Cur**)*

After the formation of **GCPLL** MLWVs in cell culture medium at pH 7 (once the solution becomes cloudy), an aliquot (10 µL) of **Cur** from 13.5 mM stock solution prepared in absolute ethanol is added to 1 mL of GCPLL solution to reach the final concentration 135 µM. After vortexing, the suspension is centrifuged at 3000 rpm for 5 min to collect a pellet of **GCPLL-Cur** MLWVs and remove the excess, non-encapsulated, **Cur** in the supernatant. The pellet is resuspended in fresh cell culture medium by vortexing.

*Encapsulation of Doxorubicin, Paclitaxel and Docetaxel*

As described for Curcumin in the previous paragraph, an aliquot (10 µL) of drug (Doxorubicin: 1 mg/ml in DMSO; Paclitaxel: 0.1 mg/ml in ethanol; Docetaxel 0.1 mg/ml in ethanol) were added to **GCPLL** MLWVs following the same protocol of centrifugation and resuspension in fresh cell culture medium by vortexing.

*Characterization of the drug loading*

The loading capacity (LC %) expressed as a percentage is the ratio:  quantity of encapsulated drugs (**Cur**) over the total amount of the delivery vehicles, in this case the weight of **GCPLL** MLWVs.

The encapsulation efficiency (EE %) is calculated by dividing the amount of encapsulated drug by the total amount of drug used during the encapsulation process, expressed as a percentage.

*Labelling of **GCPLL** and **GCPLL-Cur** with rhodamine (**GCPLL-Rhod** and **GCPLL-Rhod-Cur**)*

Both **GCPLL** and **GCPLL-Cur** MLWVs are prepared as described above. To their corresponding solution, an aliquot of 10 µL of 18:1 Liss-Rhod PE in ethanol (4 mg/mL, 3.08 mM) is added to the mixture solution so that the molar **GC**:rhodamine ratio is 200:1. After vortexing, the solution is centrifuged at 3000 rpm for 5 min and the pink pellet is resuspended in fresh cell culture media. 18:1 Liss-Rhod PE is a standard dye labelling lipid bilayers as its lipid backbone intercalates in the lipid bilayer without any perturbation, when the lipid:dye molar ratio ≥100.[5,6]

*Small Angle X-Ray Scattering (SAXS)*

pH-resolved *in situ* SAXS experiments are performed at room temperature on the Swing beamline at Soleil Synchrotron (Saint-Aubin, France) during the proposal N° 20190961. The beam energy is E= 12 keV and the sample-to-detector (Eiger X 4M)

distance is 1.995 m. Silver behenate (d(100) = 58.38 Å) is used as standard to calibrate the q-scale. Raw data collected on the 2D detector are integrated azimuthally using the in-house Foxtrot software, provided at the beamline and so to obtain the typical scattered intensity I(q) profile, with q being the wavevector ($q = (4\pi \sin\theta)/\lambda$, where $2\theta$ is the scattering angle and $\lambda$ is the wavelength). Defective pixels and beam stop shadow are systematically masked before azimuthal integration. Absolute intensity units are determined by measuring the scattering signal of water ($I_{H2O}$= 0.0163 cm$^{-1}$). SAXS profiles are processed with SasView software, version 3.1.2, available at the developer's website (sasview.org).

The experimental setup is reproduced from the Ref. [4] as follows. The sample solution (V= 1 mL, $C_{GC}$= $C_{PLL}$= 2.5 mg/mL) in DMEM and pH ~11 is contained in an external beaker under stirring at room temperature (T= 23 ± 2°C). The solution is continuously flushed through a 1 mm glass capillary using an external peristaltic pump. The pH of the solution in the beaker is changed using an interfaced push syringe, injecting microliter amounts of a 0.5 M HCl solution. pH is measured using a micro electrode (Mettler-Toledo) and the value of pH is monitored live and manually recorded from the control room via a network camera pointing at the pH-meter located next to the beaker in the experimental hutch. Considering the fast pH change kinetics, the error on the pH value is ± 0.5.


*Polarized Light Microscopy (PLM)*

PLM images are obtained with a transmission Zeiss AxioImager A2 POL optical microscope. A drop of the given sample solution was deposited on a glass slide covered with a cover slip. The microscope is equipped with a polarized light source, crossed polarizers and an AxioCam CCD camera.


*$^1$H solution nuclear magnetic resonance (NMR)*

$^1$H solution NMR experiments of the various samples are recorded on an AVANCE III Bruker 300 NMR spectrometer using standard pulse programs and a 5 mm $_1$H-X BBFO probe. The number of transients is 32 with 7.3 s recycling delay, an acquisition time of 2.73 s, and a receiver gain of 322. Chemical shifts are reported in parts-per-million ($\delta$, ppm) and referenced to the 3-(Trimethylsilyl)propionic-2,2,3,3-d$_4$ acid sodium salt (TMSP-d$_4$) (Sigma-Aldrich) peak at 0 ppm at 1 mg/mL (5.8 mM). All samples are prepared by the protocol described above. We have employed a 5 mm NMR tube containing 500 µL of solution. This solution is obtained by solubilizing the pellet of MLWVs GCPLL in MeOD. This pellet is obtained by centrifugation during 5 min at 3000 rpm. The signals that have been used for calculations are: $\delta$ (PLL) = 2.8 ppm (t) and $\delta$

(GC) = 2.25 ppm (t). All experiments were performed under the same conditions. (Figures S2-S5).

*Dynamic light scattering (DLS) and Zeta potential measurements*

Dynamic light scattering measurements (DLS) DLS experiments are performed using a Malvern Zetasizer Nano ZS90 (Malvern Instruments Ltd, Worcestershire, UK) equipped with a 4 mW He–Ne laser at a wavelength of 633 nm. Measurements were made at 25 °C with a fixed angle of 90° and three acquisitions per sample.

*Cell viability assay*

The impact of GCPLL on cell viability is first assessed using the cell line L929 of mouse fibroblasts to determine the optimal dose enabling optimal cell viability. For this purpose, $5x10^4$ cells/mL are seeded in wells of a 24 well plate and cultivated for 24 hours. Then, different GCPLL MLWV concentrations up to 250 µg/ml (when samples are centrifuged, the maximum concentration administered is 122.5 µg/ml, based on NMR data, as discussed in the text) are added to the fibroblasts L929. Cells are cultivated with GCPLL for another 24-hour period. Besides, fibroblasts are also cultivated in presence of free G-C18:1, PLL and DMEM impacted by pH changes. L929 fibroblasts cultivated in complete medium are used as control samples.

Cell viability is determined by measuring the metabolic activity using Alamar Blue assay. Basically, GCPLL particles are taken out from the wells and L929 cells are rinsed twice with fresh medium. Then, 300 µL of a resazurin solution at 0.01 % (w/v) in colourless fresh DMEM medium is added to cells and incubated for 4 hours. The supernatant in each well is then collected, diluted with 700 µL of fresh medium, and the absorbance measured at $\lambda$ = 570 nm and $\lambda$ = 600 nm. The percentage of resazurin reduction is calculated following the formula provided by the supplier. Cell metabolic activity of the samples is compared to control samples. The arbitrary value 100 % is given to controls.

After determination of the optimal dose, the antiproliferative activity of GCPLL, GCPLL-Cur and Cur is assessed for 3 different human cell lines: Hela, Normal Human Dermal Fibroblasts (NHDF) and macrophage derived THP-1 cells.

HeLa and NHDF are seeded 24 hours prior to the experiment in 24-well plates with a density of $5x10^4$ cells/ml and grown under standard conditions (DMEM medium supplemented with 10% fetal bovine serum, 1% penicillin/streptomycin and 1% Anphotericin B at 37˚C, 5% $CO_2$ and 90% humidity). Non adherent THP-1 cells are seeded at a density of $4x10^5$ cells/mL in wells and incubated for 24 hours with PMA 10 µg/mL in deprived RPMI 1640 medium to differentiate them into adherent macrophage

5

like cells. Then, the cell culture media was replaced by fresh complete RPMI 1640. After 24 hours in culture, the different concentrations of particles are administered to the cells and cells cultured for another 24h. The Alamar Blue colorimetric assay is used for cell viability evaluation for all types of cells as previously described.

*Optical fluorescence microscopy*

5 x$10^4$ cells/well are seeded into a 6 well-plate and grown under standard conditions as previously described. After 24 h, solutions of GCPLL and GCPLL-Cur, analogously GCPLL-Rhod and GCPLL-Rhod-Cur are added at the final concentration of 100 $\mu$g/mL and incubated for another 24 h period. Then, samples are rinsed 3 times with PBS, fixed for 1 hour by adding 1 mL of 4% PFA in PBS. After 3 rinses with PBS, cells are incubated for 15 min in a solution of PBS-Tween at 0.2% to permeabilize them. Then, 300 $\mu$L/well of DAPI (1/50000) are added and cells incubated for 10 min. Last cells are rinsed 3 times with PBS and kept at 4°C protected from the light until analysis. Cells are observed using a ZEISS fluorescence microscope, equipped with camera AxioCam MRm.

*Flow Cytometry Analysis*

1x$10^5$ cells/well are seeded into a 6 well-plate, cultivated for 24 h, then treated with MLWV particles using a concentration of 100 $\mu$g/mL and incubated for another 24 h. Samples for Facs analysis are obtained by detaching cells with 300 $\mu$L/well of trypsin for approximately 5 min, and collected within 1 mL of cell culture medium in microfuge tubes. Detached cells are collected in tubes and are centrifuged at 300 g for 5 min. After supernatant removal, the pellet is resuspended in 1 mL of PBS containing 0.5% paraformaldehyde (PFA).
Flow Cytometry is performed on a CELESTA SORP flow cytometer (BD Biosciences, Franklin Lakes, NJ, USA). Acquisition gate is set to record $10^5$ events total for each sample.

*Confocal laser scanning microscopy*

Samples are prepared using the same protocol than that for regular fluorescence microscopy, except cells are cultured in a Thermo Scientific™ Nunc™ Lab-Tek™ II Chamber Slide™ with 2 wells for an optimal visualization.

Analyses are performed in a spinning-disk head X1 (Yokogawa) mounted on a Nikon Eclipse Ti inverted microscope. Cells are observed with a 60x/1.4 Plan Apo objective and a Hamamatsu Orca Flash SCMOS camera.

*References*

1    N. Baccile, M. Selmane, P. Le Griel, S. Prévost, J. Perez, C. V. Stevens, E. Delbeke, S. Zibek, M. Guenther, W. Soetaert, I. N. A. Van Bogaert and S. Roelants, *Langmuir*, 2016, **32**, 6343–6359.

2    S. R. Lewis, S. Datta, M. Gui, E. L. Coker, F. E. Huggins, S. Daunert, L. Bachas and D. Bhattacharyya, *Proc. Natl. Acad. Sci.*, 2011, **108**, 8577–8582.

3    C. Seyrig, P. Le Griel, N. Cowieson, J. Perez and N. Baccile, *J. Colloid Interface Sci.*, 2020, **580**, 493–502.

4    C. Seyrig, G. Kignelman, W. Thielemans, P. Le Griel, N. Cowieson, J. Perez and N. Baccile, *Langmuir*, 2020, **36**, 8839–8857.

5    A. I. Novaira, V. Avila, G. G. Montich and C. M. Previtali, *J Photochem Photobiol B*, 2001, **60**, 25–31.

6    M. Leonard-Latour, R. M. Morelis and P. R. Coulet, *Langmuir*, 1996, **12**, 4797–4802.
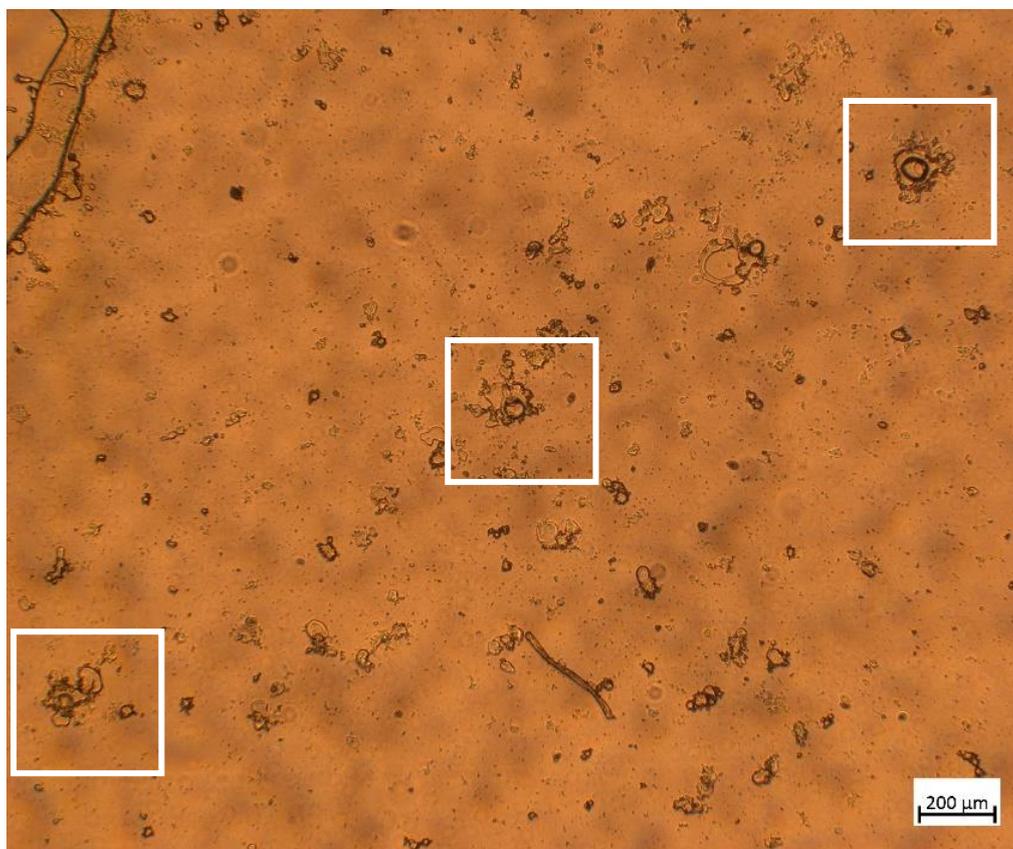
Figure S1. PLM images of GCPLL 2.5 mg/mL in DMEM cell culture media containing birefringent patterns on the surface evidenced by rotating the polarizers from 45°–135° (b) to 0–90°(c).
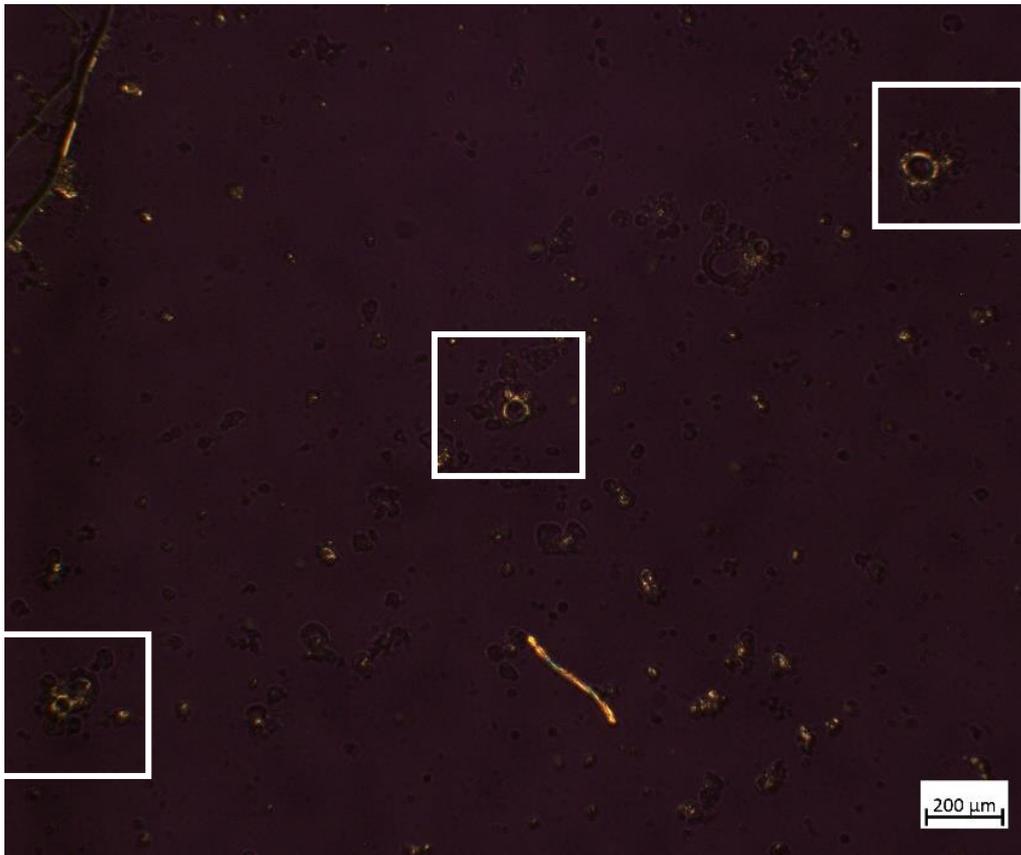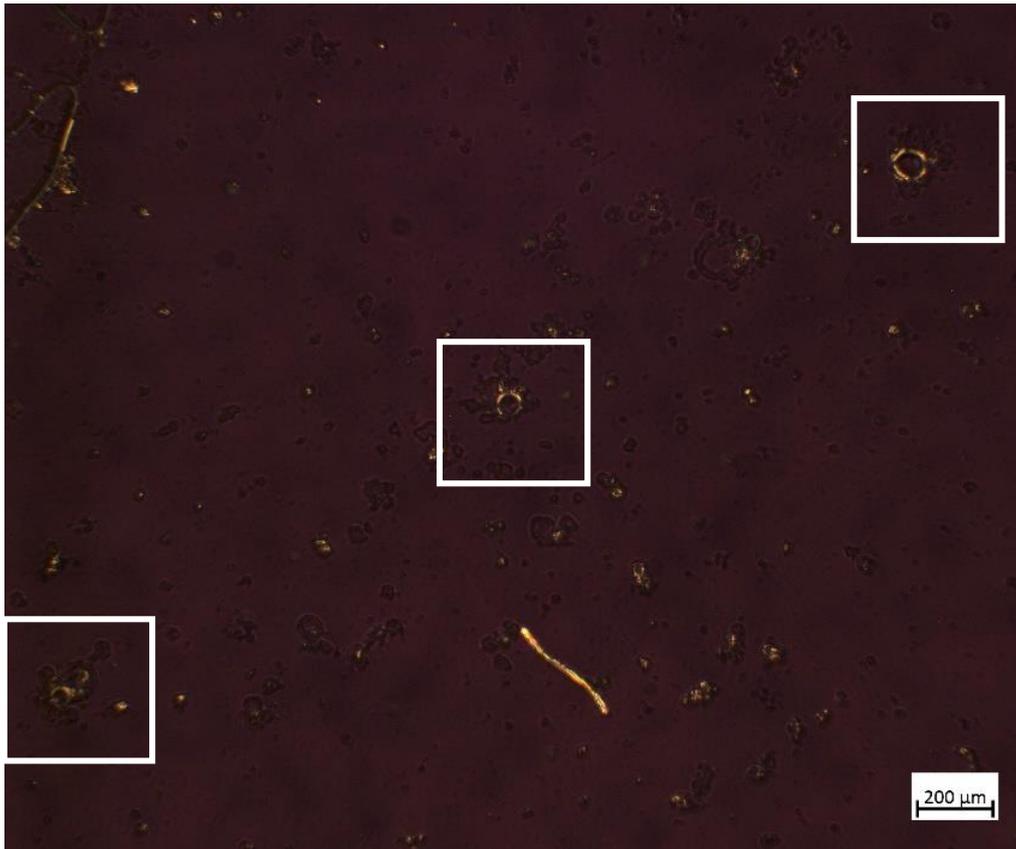
Figure S1 *continued*. PLM images of GCPLL 2.5 mg/mL in DMEM cell culture media containing birefringent patterns on the surface evidenced by rotating the polarizers from 45°–135° (b) to 0–90°(c).
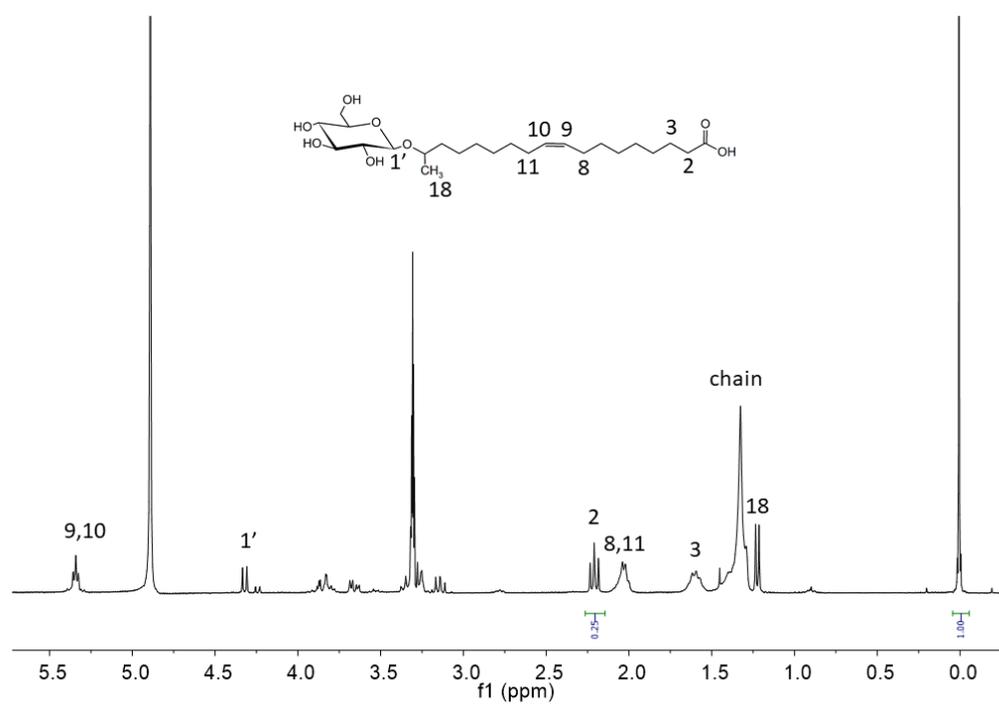
Figure S2. $^1$H NMR of control GC in methanol-d$_4$.

.
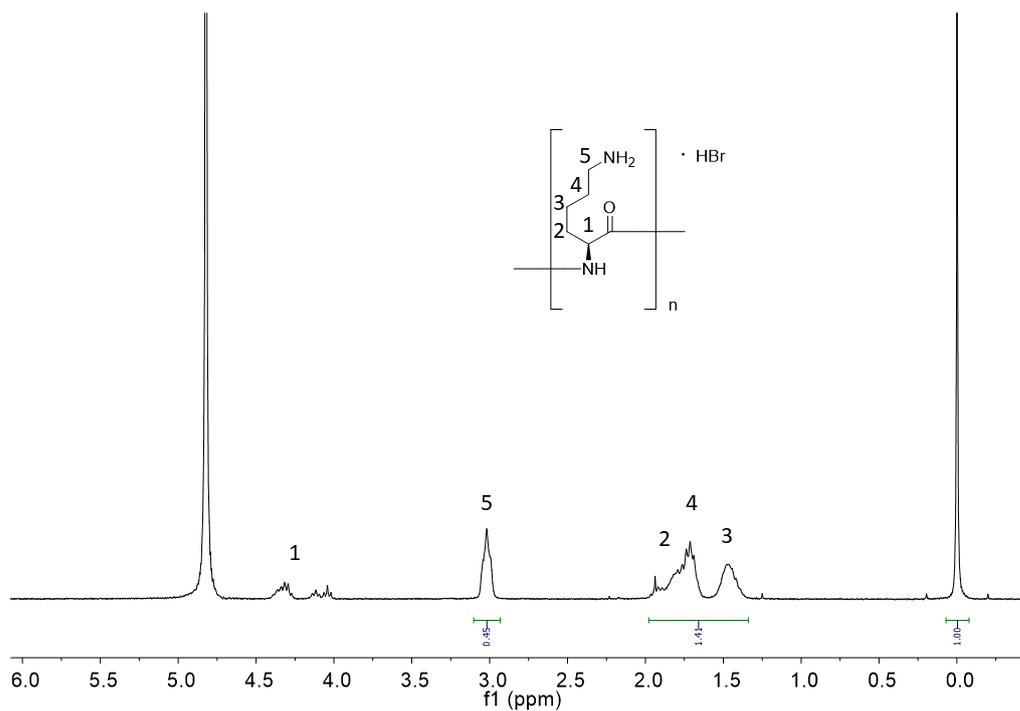
Figure S3. $^1$H NMR of control PLL in D$_2$O.
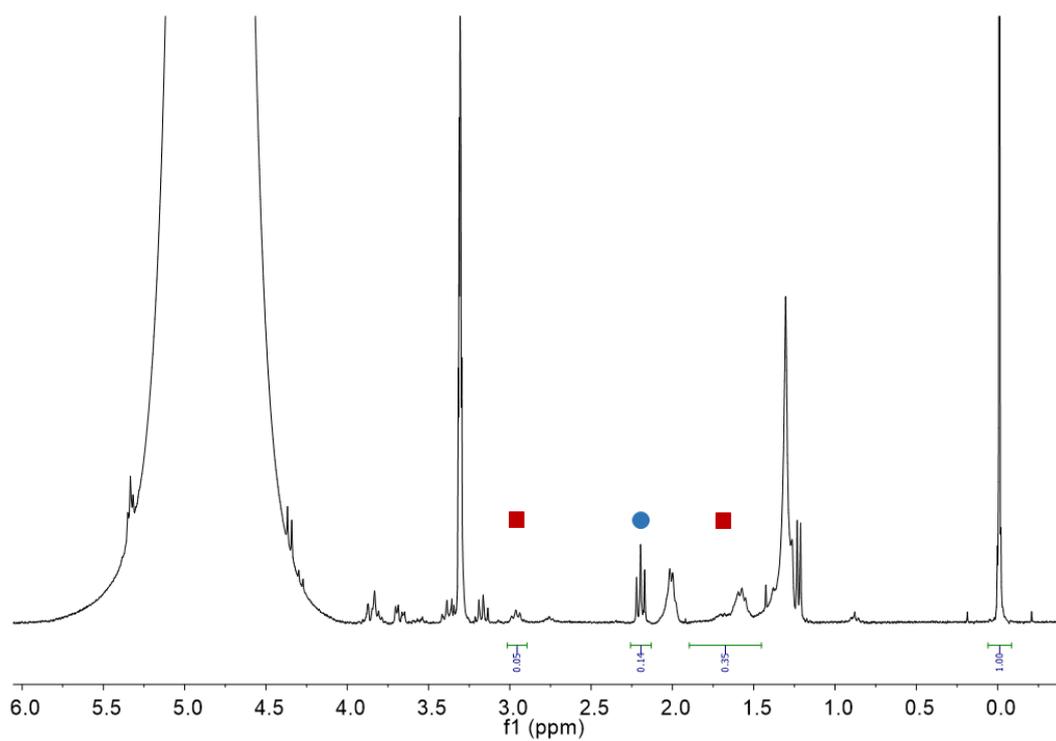


Figure S4. $^1$H NMR from sample GCPLL in H$_2$O, centrifuged pellet and dissolved in methanol-d$_4$, where peaks assigned with ■ and ● correspond to PLL and GC, respectively.
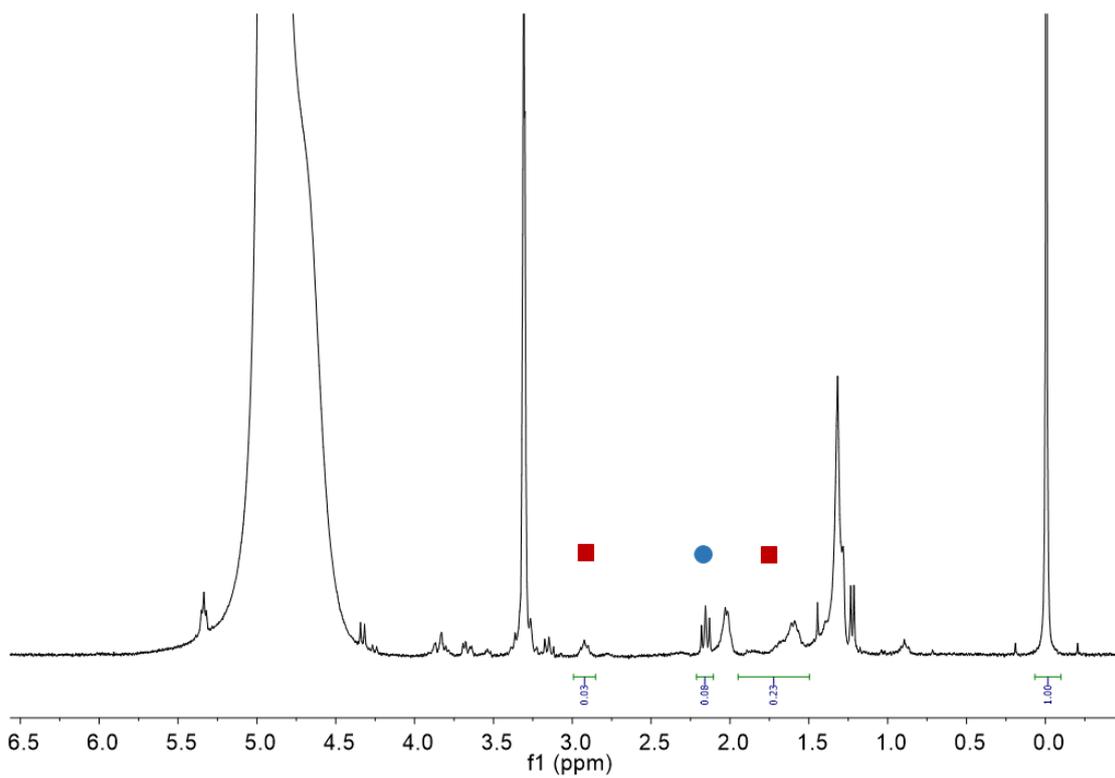
Figure S5 $^1$H NMR from sample GCPLL in DMEM, centrifuged and dissolved in methanol-d$_4$, where peaks assigned with ■ and ● correspond to PLL and GC, respectively.

**Table S1.** Quantitative analysis of the integrals corresponding to the $^1$HNMR spectra of the GCPLL prepared in $H_2O$ (pH 5) and DMEM cell culture media (pH 7.5) and the resulting pellet dissolved in MeOD-$d_4$, shown in Figures S2-5. PLL is represented by the $(RC\underline{H}_2NH_2)_x$ (where $x\sim20$) peak at $\delta=2.8$ ppm. The $M$w (PLL)$\approx$1-5KDa, then we consider an average $M$w (PLL)=2.5kDa, whereas the $M$w of each monomer is 128 g/mol, yielding an average of 20 monomers per PLL chain. The valence of the $(RC\underline{H}_2NH_2)_x$ ($x\sim$ 20) peak is then taken as 40. G-C18:1 is represented by the $RC\underline{H}_2C=O$ peak at $\delta=2.2$ppm. The $M$w (G-C18:1)=460g/mol and each G-C18:1 bears a single COOH group. The valence of the $RC\underline{H}_2C=O$ peak is then taken as 2. The peak at $\delta=0$ ppm corresponds to the reference (TMSP-$d_4$,1mg.mL$^{-1}$ $\equiv$ 5.8mM), having a valence of 9.

| | Integrals | | | $C_{initial}$ (mM) | | $C_{final}$ (mM) | | $C_F/C_{In}$ (%) | | Molar ratio | | Functional group |
|---|---|---|---|---|---|---|---|---|---|---|---|---|
| | GC (2H) | PLL (40H) | TMSP-d4 (9H) | $[GC]_{in}$ | $[PLL]_{in}$ | $[GC]_f$ | $[PLL]_f$ | $GC_{f/in}$ | $PLL_{f/in}$ | $GC_{in}/$ $PLL_{in}$ | $GC_f/$ $PLL_f$ | $[COOH]/$ $[NH_2]$ |
| $H_2O$ | 0.14 | 0.05 | 1 | 5.4 | 1 | 3.7 | 0.065 | 70 | 6.5 | 5.4 | 57 | 2.8 |
| DMEM | 0.09 | 0.03 | 1 | 5.4 | 1 | 2.4 | 0.04 | 45 | 4 | 5.4 | 60 | 3 |
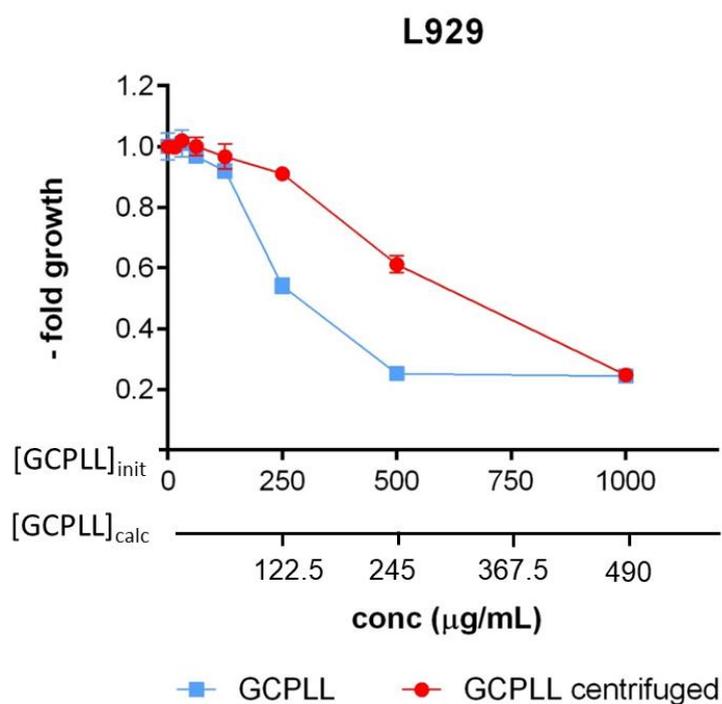
**L929**



Figure S6. Cell viability comparison of both GCPLL and GCPLL centrifugated at 3000 rpm during 5 min and resuspended with new cell culture media on L929 fibroblasts mouse cell line. [GCPLL]$_{calc}$ refers to the concentration of GCPLL centrifuged calculated by 1H NMR described in Table S1.
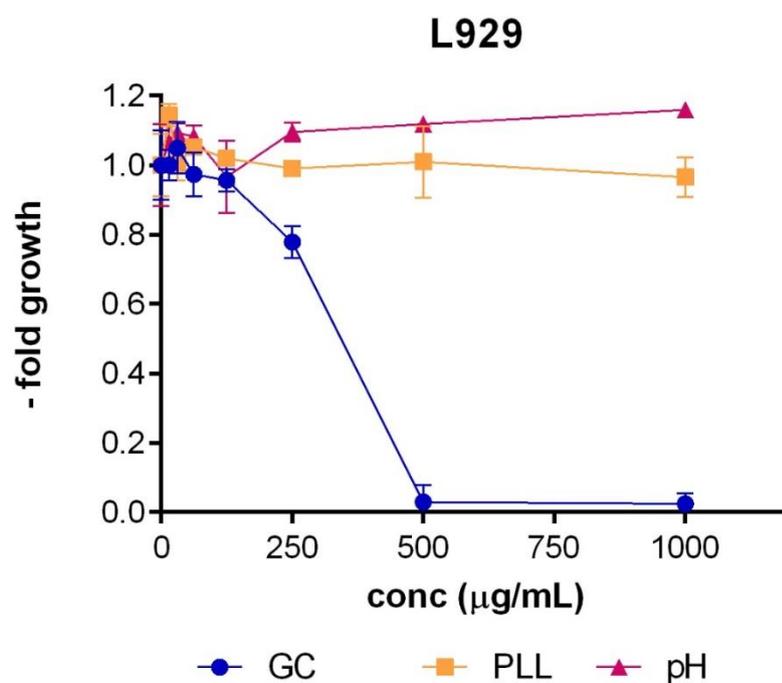
**L929**



Figure S7. Cell viability of DMEM cell culture medium altered with changes in pH, glucolipid GC18:1 (GC) and poly-L-lysine (PLL) on L929 fibroblasts mouse cell line.
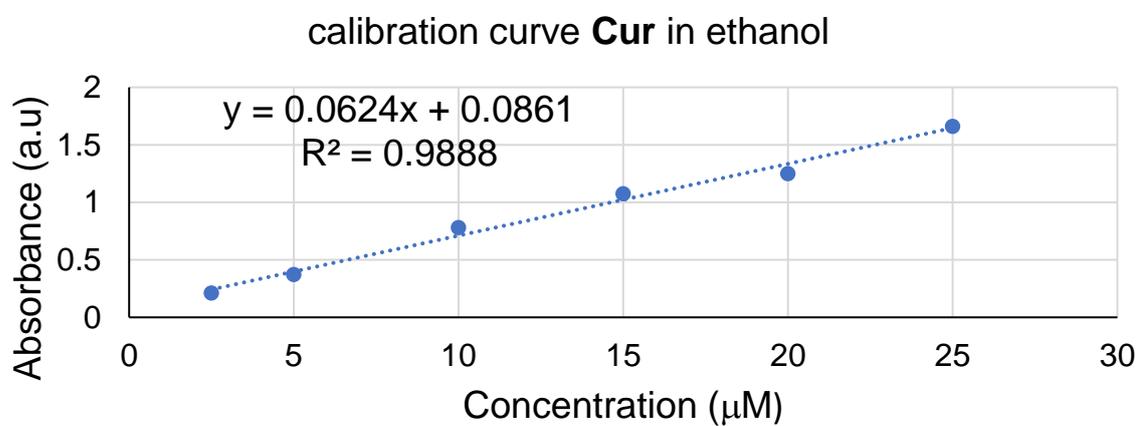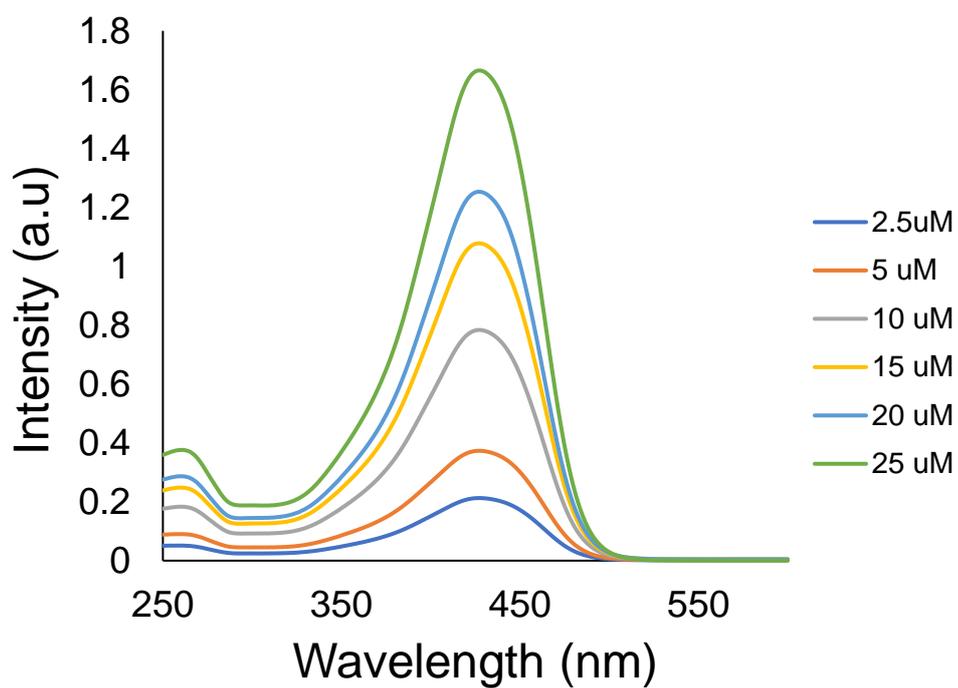
Figure S8. UV-Vis spectra of the calibration curve of Curcumin in ethanol.

Control

GCPLL

Curcumin

GCPLL- Cur
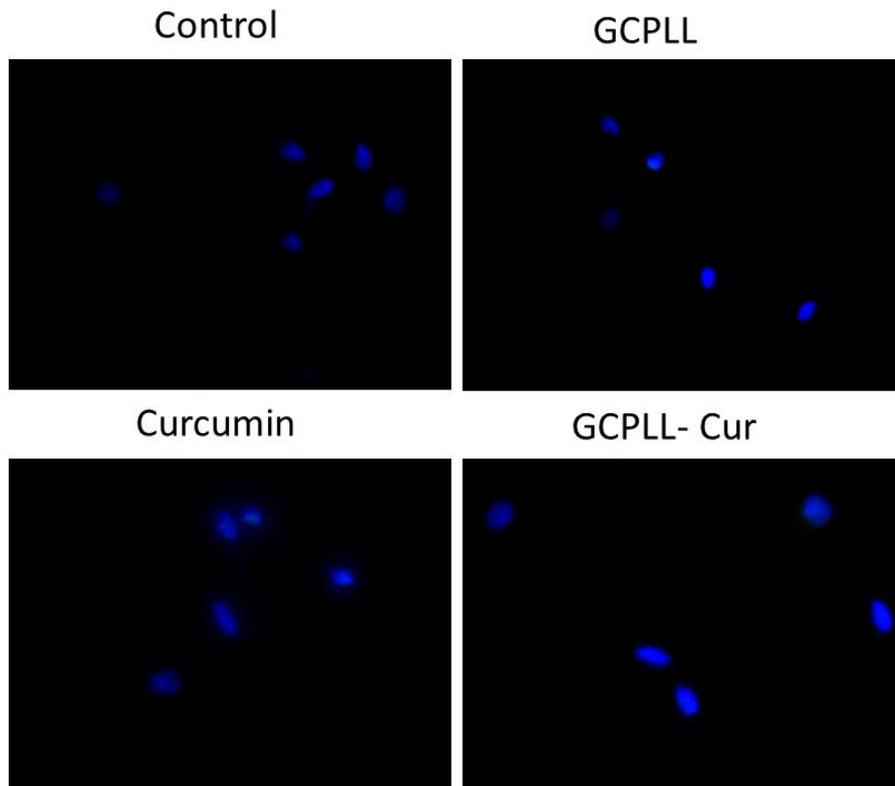
Figure S9. Fluorescence microscopy of **NHDF** cells stained with DAPI dye for nucleus.

control

GCPLL-LisRhod

Cur + LisRhod

GCPLL-Cur-LisRhod
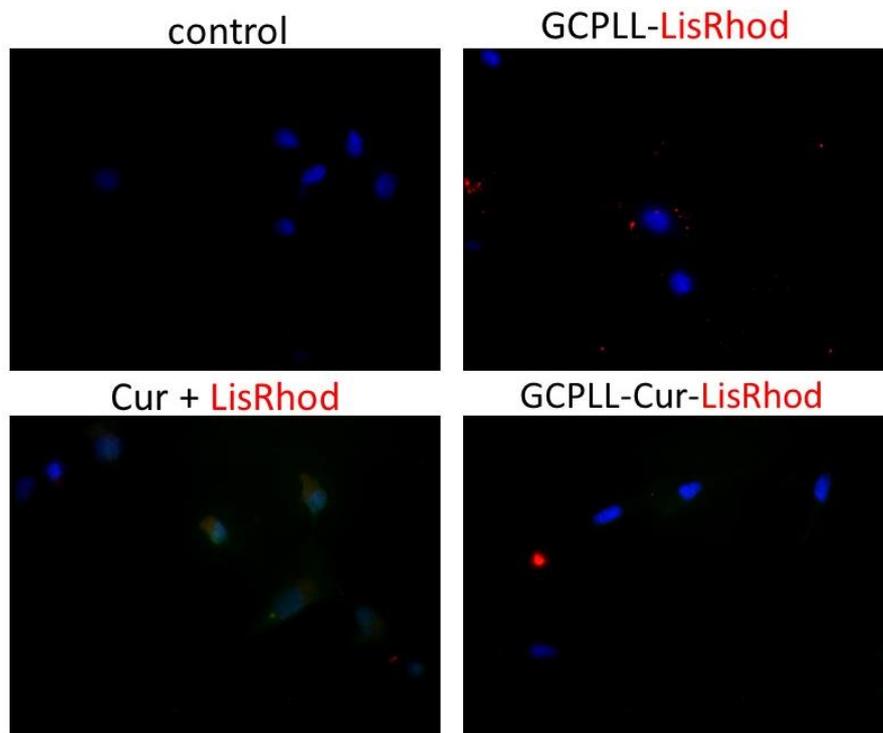
Figure S10. Fluorescence microscopy of **NHDF** cells stained with DAPI dye for nucleus and GCPLL labelled with Rhodamine-lipid (Liss-Rhod).
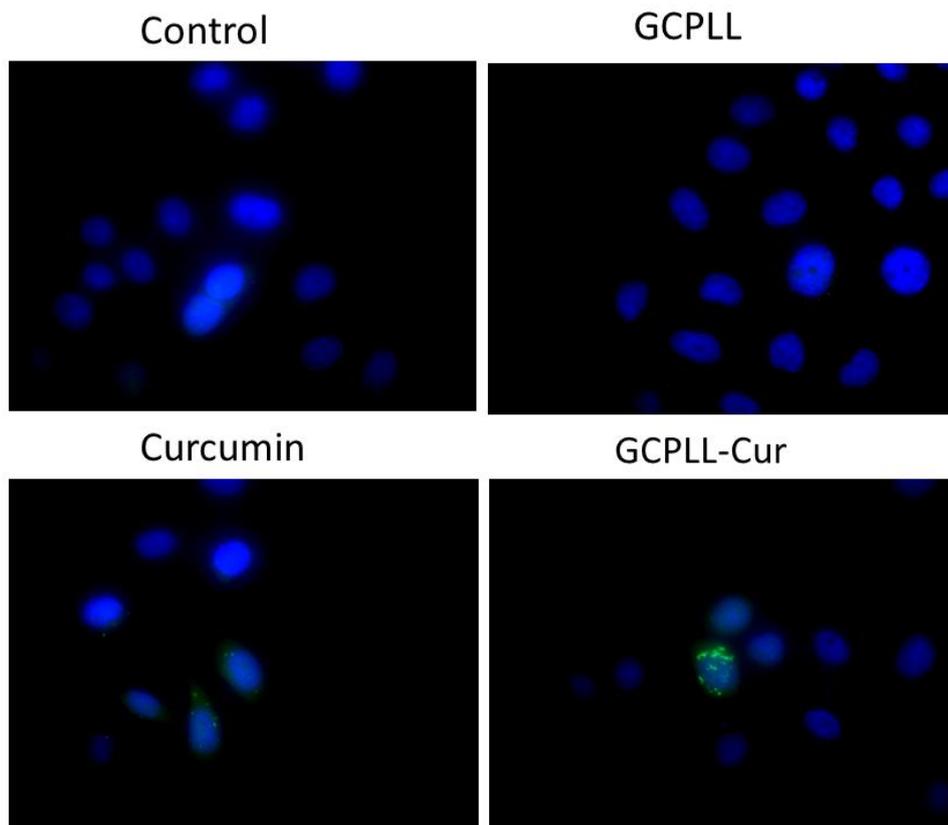
Figure S11. Fluorescence microscopy of **Hela** cells stained with DAPI dye for nucleus.
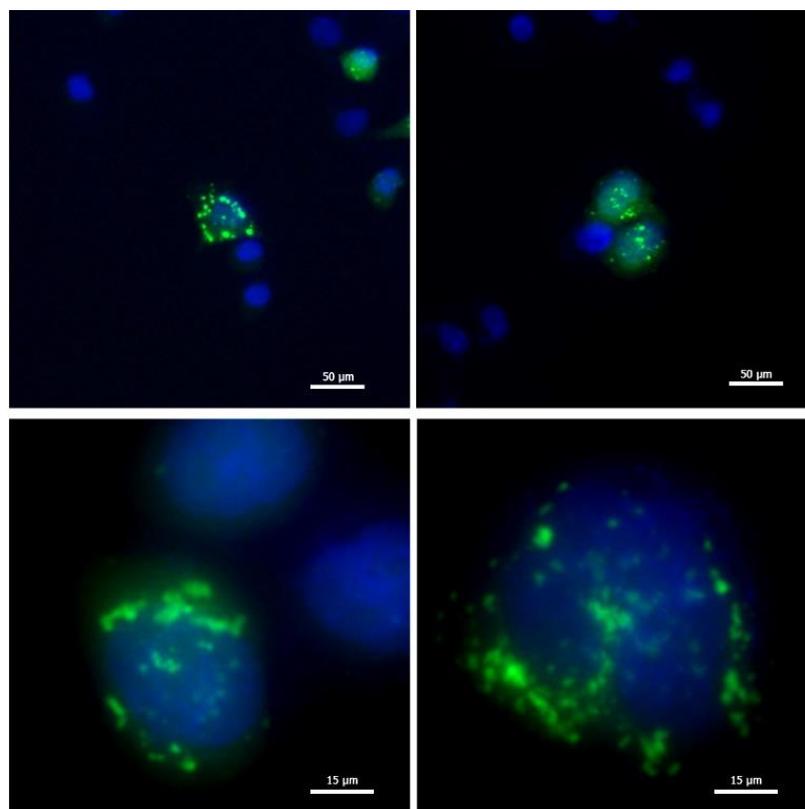


Figure S12. Fluorescence microscopy zoom images of **Hela** cells stained with DAPI dye for nucleus after administration with GCPLL-Cur.
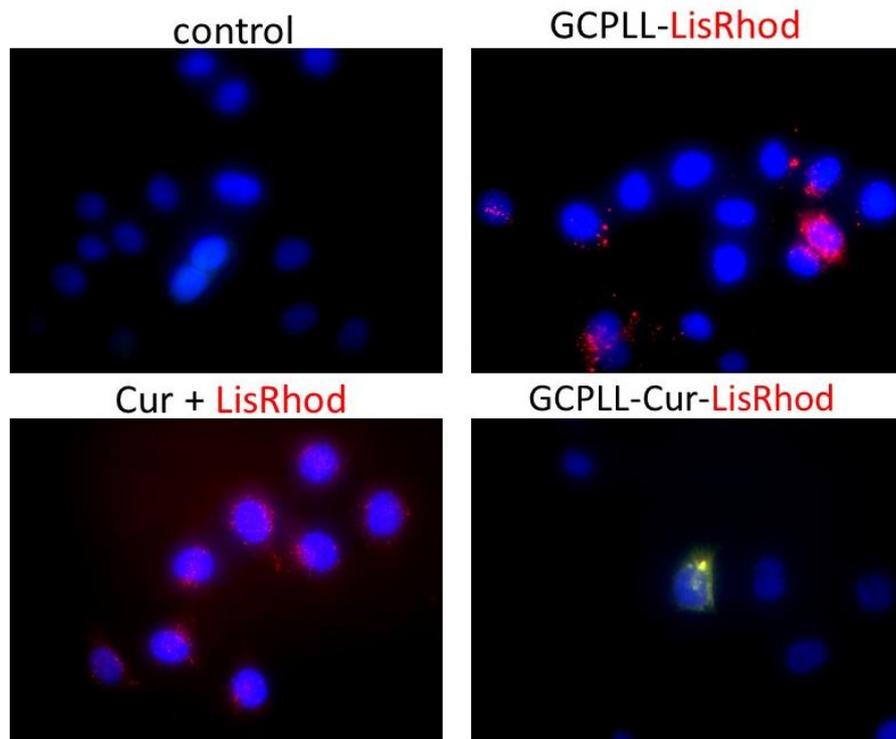
Figure S13. Fluorescence microscopy of **Hela** cells stained with DAPI dye for nucleus and GCPLL labelled with Rhodamine-lipid (Liss-Rhod).
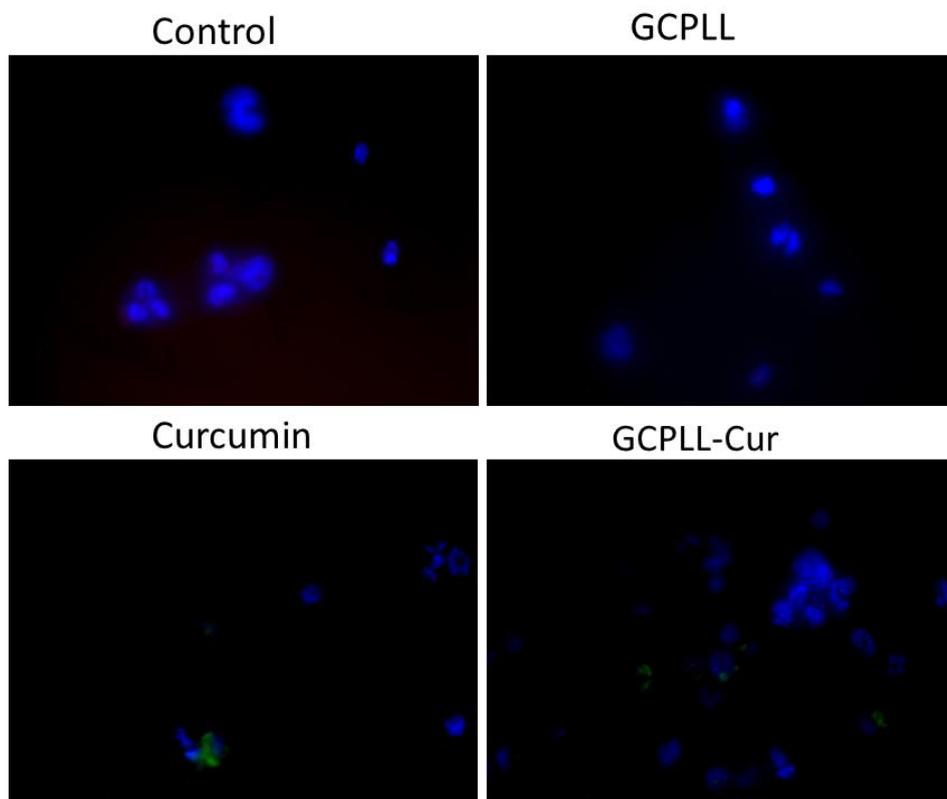


Figure S14. Fluorescence microscopy of **THP-1** cells stained with DAPI dye for nucleus.
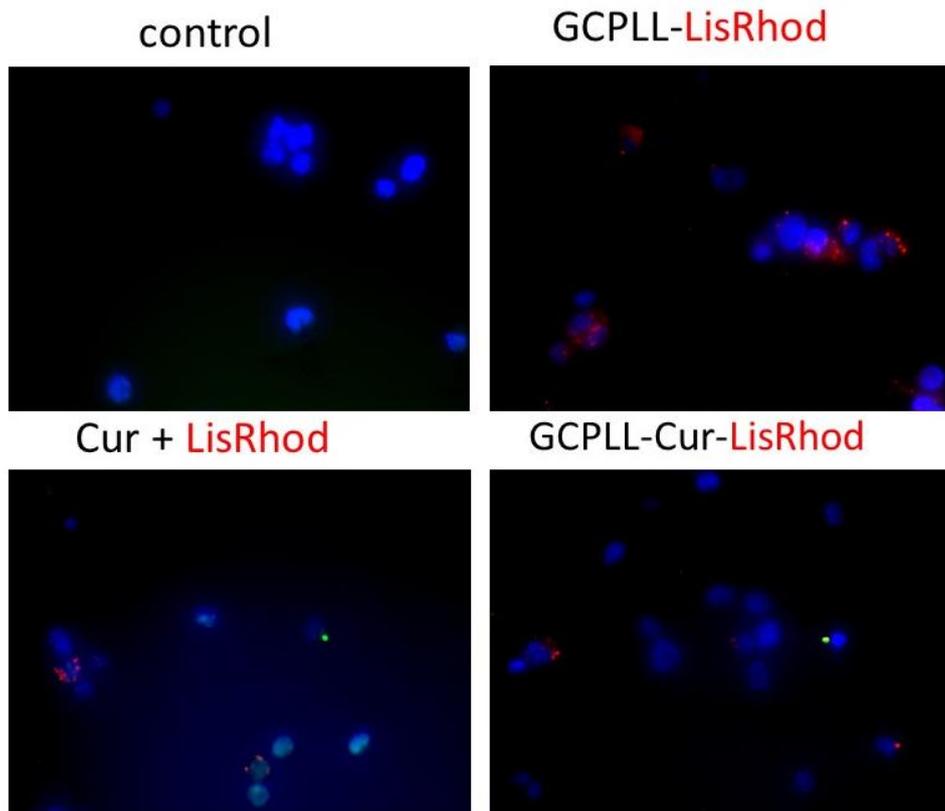
Figure S15. Fluorescence microscopy of **THP-1** cells stained with DAPI dye for nucleus and GCPLL labelled with Rhodamine-lipid (Liss-Rhod).
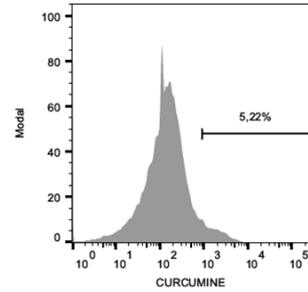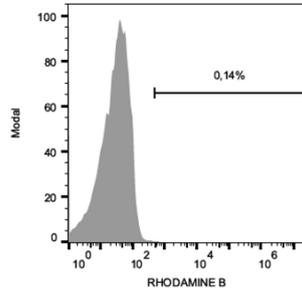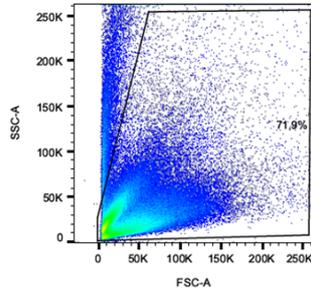
HeLa
blank



HeLa
GCPLL-Rhod
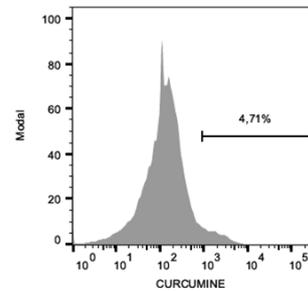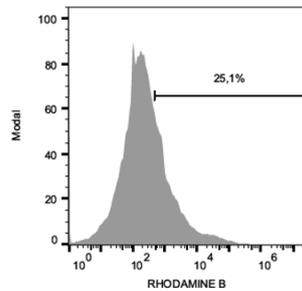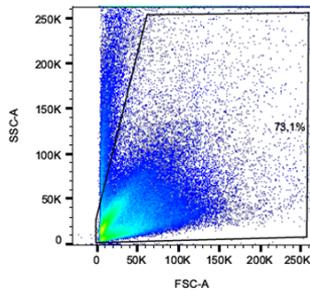


HeLa
GCPLL-Rhod-Cur
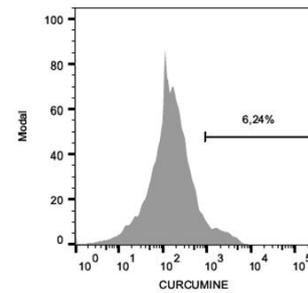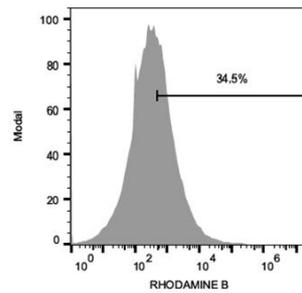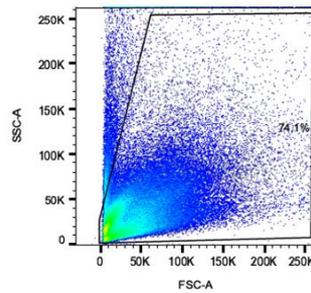


Figure S16. Flow cytometry raw data examples of the triplicate experiments with 3 replicates each one in Hela cells, for: blank; GCPLL-Rhod and GCPLL-Rhod-Cur.
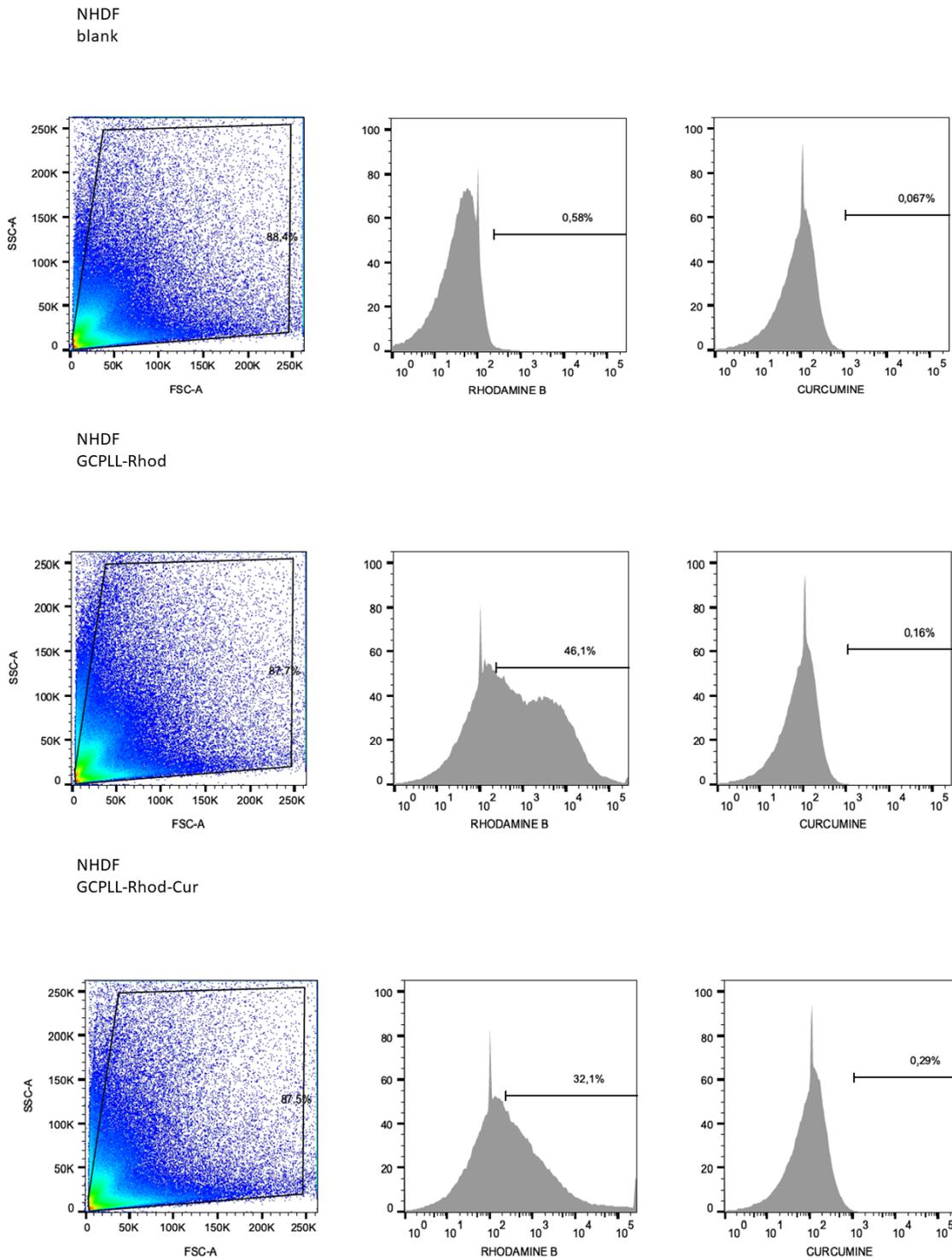
Figure S17. Flow cytometry raw data examples of the triplicate experiments with 3 replicates each one in NHDF cells, for: blank; GCPLL-Rhod and GCPLL-Rhod-Cur.

THP-1
blank
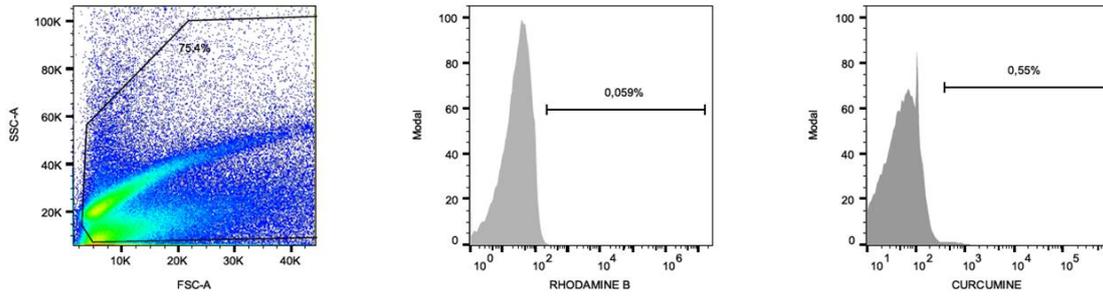


THP-1
GCPLL-Rhod
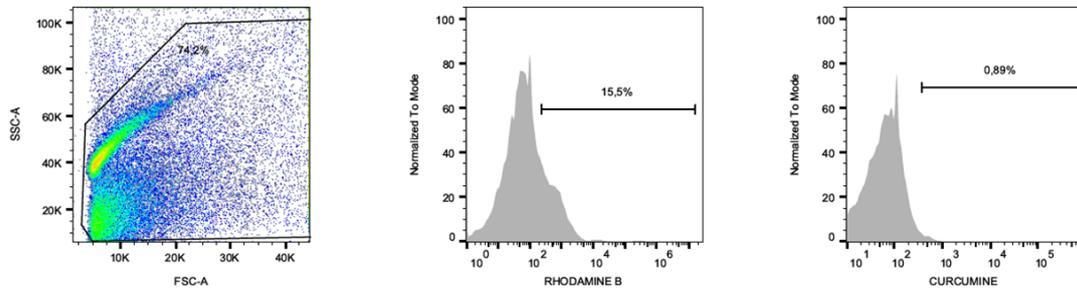


THP-1
GCPLL-Rhod-Cur
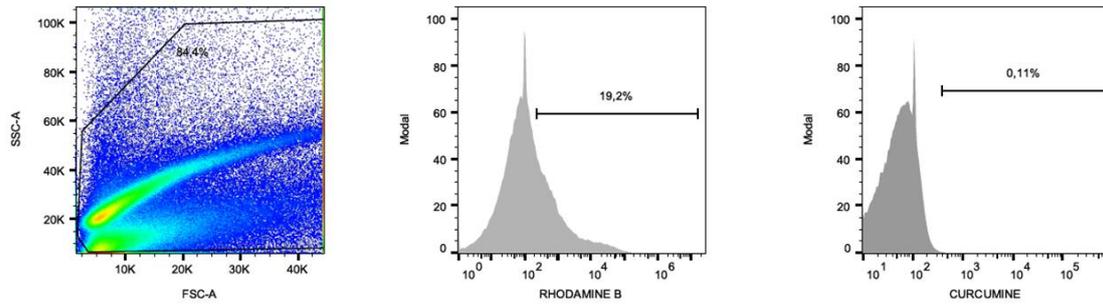


Figure S18. Flow cytometry raw data examples of the triplicate experiments with 3 replicates each one in THP-1 cells, for: blank; GCPLL-Rhod and GCPLL-Rhod-Cur.
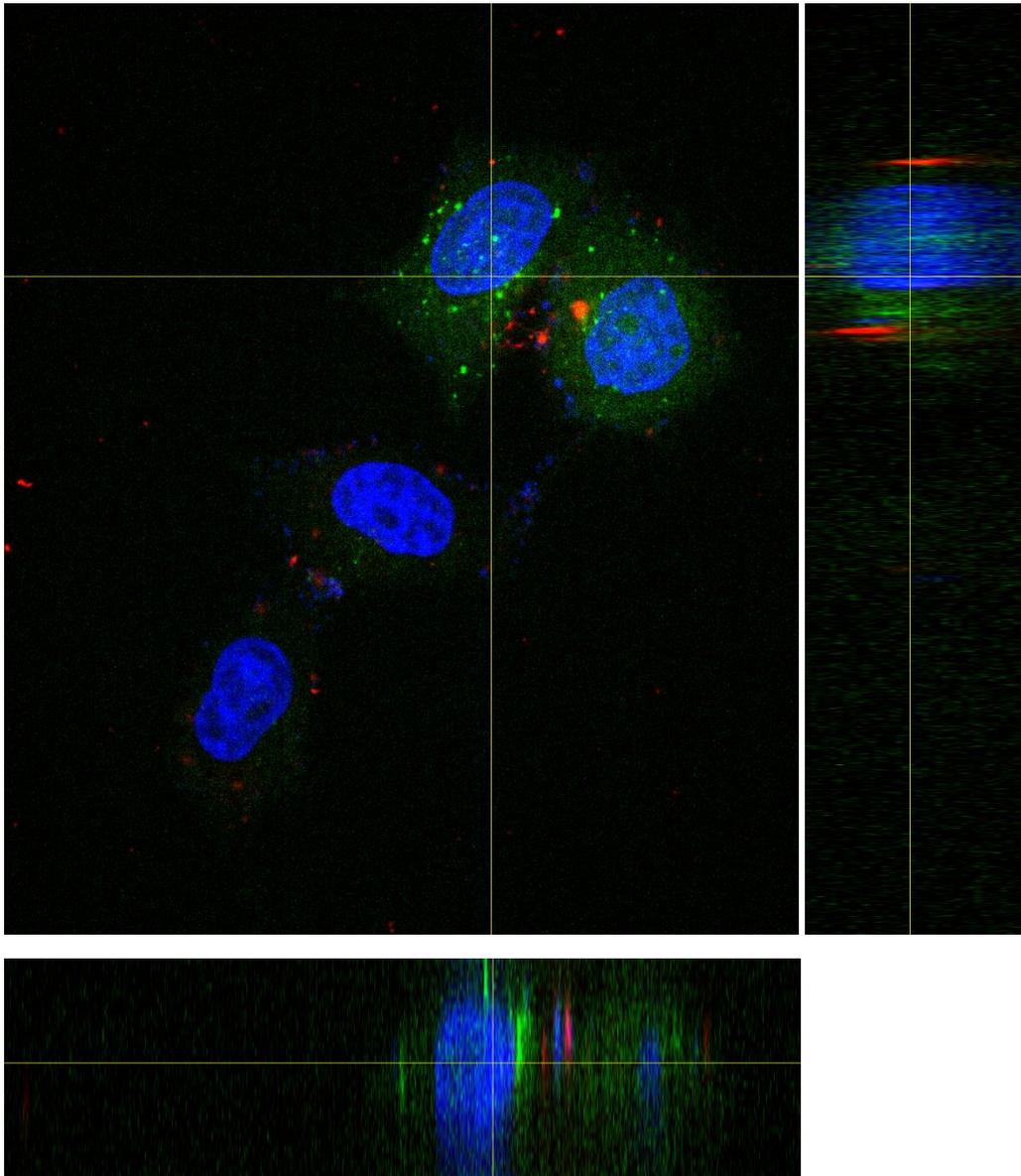
Figure S19. Orthogonal views of confocal microscopy images